TITLE

Single-cell profiling of complex plant responses to *Pseudomonas syringae* infection

AUTHORS

Jie Zhu[1], Signe Lolle[1], Andrea Tang[1], Bella Guel[1], Brian Kvikto[2], Benjamin Cole[3,4*], Gitta Coaker[1*]

AUTHOR AFFILIATIONS

[1]Department of Plant Pathology, University of California, Davis, Davis, CA, 95616, USA

[2]Department of Plant Pathology, University of Georgia, Athens, GA, 30602, USA

[3]DOE-Joint Genome Institute, Berkeley, CA, 94720, USA

[4]Lawrence Berkeley National Laboratory, Berkeley, CA, 94720, USA

CONTACT INFORMATION

Correspondence: bjcole@lbl.gov and glcoaker@ucdavis.edu

SUMMARY

Plant response to pathogen infection varies within a leaf, yet this heterogeneity is not well resolved. We exposed *Arabidopsis* to *Pseudomonas syringae* or mock treatment and profiled >11,000 individual cells using single-cell RNA sequencing. Integrative analysis of cell populations from both treatments identified distinct pathogen responsive cell clusters exhibiting transcriptional responses ranging from immunity to susceptibility. Pseudotime analyses through pathogen infection revealed a continuum of disease progression from an immune to susceptible state. Confocal imaging of promoter reporter lines for transcripts enriched in immune cell clusters expressed surrounding substomatal cavities colonized or in close proximity to bacterial colonies, suggesting cells within immune clusters represent sites of early pathogen invasion. Susceptibility clusters exhibited more general localization and were highly induced at later stages of infection. Overall, our work uncovers cellular heterogeneity within an infected leaf and provides unique insight into plant differential response to infection at a single-cell level.

KEYWORDS

Single-cell RNA-seq, *Pseudomonas syringae*, disease susceptibility, plant innate immunity, heterogeneous infection

INTRODUCTION

Plants can be infected by diverse pathogens capable of colonizing roots, vascular tissues, and foliar (leaf) tissue. Many plant diseases exhibit variable symptoms. For example, inoculation of bacteria or fungal spores using spray or infiltration results in unequal symptom development and a relatively small proportion of pathogens successfully invade their hosts (Berruyer et al., 2006; Pétriacq et al., 2016; Xin et al., 2016). Moreover, different stages of pathogen infection are often observed within a leaf (Fantozzi et al., 2021; Haueisen et al., 2019). Heterogeneity in pathogen distribution and likely, the plant response, impacts symptom development (Matsumoto et al., 2022). Strains of the bacterial pathogen, *Pseudomonas syringae*, have a broad host range and can infect many economically important plant species, causing a variety of foliar symptoms (Katagiri et al., 2002; Xin et al., 2018).

Mechanisms regulating pathogen distribution and colonization on plants can be a combination of physical, metabolic and immune barriers. Physical barriers, such as trichomes, the waxy cuticle, plant cell walls and closed stomatal pores can regulate the penetration of pathogens into the plant interior (Bigeard et al., 2015; Wang et al., 2019). Plants can also recognize pathogen molecular features, induced damage and effectors using either surface-localized or intracellular immune receptors (Yuan et al., 2021). Surface-localized pattern recognition receptors (PRRs) detect microbe-associated molecular patterns (MAMPs) or damage (DAMPs) resulting in PRR-triggered immunity (PTI). Immune recognition leads to a series of downstream defense responses including calcium influx, the production of reactive oxygen species, defense hormone production and global transcriptional reprogramming (Lolle et al., 2020; Zhou and Zhang, 2020). PTI can be generally induced against diverse pathogens because of the conserved nature of MAMPs (e.g., bacterial flagellin and elongation factor Tu, fungal chitin) (Zhou and Zhang, 2020). However, virulent pathogens secrete metabolites and proteinaceous effectors that dampen immunity and establish suitable environments for growth (Toruño et al., 2016). Thus, plant-pathogen interactions are a highly dynamic process, resulting in heterogeneous cellular responses.

Past studies investigating plant-pathogen interactions mainly depend on assays from bulk tissue (i.e. whole leaf or roots). While genome-wide transcriptional profiling has advanced our understanding of immune responses, they average cellular responses across the entire tissues (Liu et al., 2022; Zipfel et al., 2006). Single-cell RNA sequencing (scRNA-seq) technologies enable massively parallel transcriptional profiling of thousands of cells (Kolodziejczyk et al., 2015; Libault et al., 2017; Macosko et al., 2015; Tang et al., 2009). scRNA-seq interrogates populations at the single-cell level and on a genome-wide scale to profile transcriptomes from different cell types and cell states (Libault et al., 2017; Seyfferth et al., 2021). The application of scRNA-seq in plants has provided new insight into cell identity, function and development in different tissues (Denyer et al., 2019; Kim et al., 2021; Lopez-Anido et al., 2021; Procko et al., 2022; Shahan et al., 2022; Zhang et al., 2019). With respect to pathogen infection, it

remains unclear how large populations of plant cells within a tissue respond and how pathogen proximity influences cellular responses at high resolution.

In this study, we combined scRNA-seq and live-cell imaging of fluorescent reporters to investigate plant cellular responses to pathogen infection. We established a transcriptome atlas of *Arabidopsis* leaf tissue infected with virulent *P. syringae*. The atlas enabled the identification of pathogen-responsive cell clusters at immune, transition and susceptible states. Pseudotime trajectory revealed a continuum of disease progression from an immune to susceptible state. We validated this trajectory using fluorescent transcriptional reporter lines expressing either immune or susceptible cell cluster markers identified by scRNA-seq. Finally, we identified diverse spatial and temporal patterns of immune and susceptible marker genes which can be influenced by pathogen proximity.

RESULTS

Single-cell RNA-seq profiling of *Arabidopsis* leaf tissue infected with *P. syringae*

To investigate plant responses to pathogen infection at high resolution, we first analyzed bacterial distribution within a leaf. Virulent *P. syringae* pv. tomato DC3000 *ΔhopQ1* labeled with 3xmCherry (*Pst* DC3000) was inoculated on four-week-old *Arabidopsis thaliana*. The *hopQ1* effector deletion strain frequently used as a tool to investigate *P. syringae,* is fully virulent on *Arabidopsis* and also infects *Nicotiana benthamiana* (Wei et al., 2007). We observed patchy distribution of *Pst* DC3000 as well as differences in colony number and area within a leaf at 24h post-infiltration (hpi), suggesting bacterial colonization is spatially variable (Figure 1A-C). At this infection stage, *Arabidopsis* leaves do not exhibit visible symptoms, but bacteria multiply aggressively (Katagiri et al., 2002; Whalen et al., 1991).

Pst DC3000 colonizes the intercellular space between mesophyll cells, manipulating them to provide more favorable conditions for microbial growth. To characterize the dynamics of the interaction between *Pst* DC3000 and *Arabidopsis* mesophyll tissue, we enriched for mesophyll cells using the Tape-*Arabidopsis* Sandwich method (Figure 1D) (Wu et al., 2009). Single-cell transcriptomes were then profiled from *Pst* DC3000- and mock-treated samples 24hpi using the 10X Genomics scRNA-seq platform (Figure 1D). We recovered 11,895 single-cell transcriptomes with a median number of 3,521 genes and 17,017 unique transcripts, representing over 80% of protein-coding genes in the *Arabidopsis* genome (Figure S1A-B). Complementing our single-cell datasets, we also performed bulk RNA-seq for protoplasts and infiltrated leaves to identify genes modulated in response to pathogen infection (n = 890; adjusted p-value < 0.01, log fold-change > 2), as well as genes possibly affected by protoplast generation (n = 7548; adjusted p-value < 0.01, log fold-change > 0.5). We excluded protoplast-inducible genes. There was a strong correlation between merged single-cell and bulk protoplasts

samples (Spearman's Rho =0.786 and 0.848 for mock- and bacteria-treated samples, respectively, Figure S1C).

Using graph-based unsupervised clustering, we identified 18 major cell clusters and visualized them on a uniform manifold approximation and projection (UMAP) plot (Figure 1E and Table S1). Each cluster contained cells from both *Pst* DC3000- and mock-treated leaves (Figure 1E and Figure S1D). To assign cell types, we utilized a recently published single-cell transcriptomics survey of *Arabidopsis* leaf tissue (Kim et al., 2021), as well as expression of well-known cell-type markers. The predominant predicted identity of cells within each cluster was then used to assign a cell type to the whole cluster. We also integrated our single-cell datasets with five previously published *Arabidopsis* leaf scRNA-seq datasets (Kim et al., 2021; Liu et al., 2020; Lopez-Anido et al., 2021; Procko et al., 2022; Zhang et al., 2021). Analysis of the integrated dataset suggests that the vast majority of cells profiled in this study are similar in cell type as those profiled by others, with the exception of an increased density of *Pst* DC3000-treated cells within the larger mesophyll cell cluster (Figure S2). The 18 cell clusters contain eight cell types, but exhibit predominant mesophyll identity (~93.7% of all cells, clusters M1 - M14, Figure 1E-F and Figure S1D).

scRNA-seq reveals cell clusters ranging from immunity to susceptibility within a leaf

Integrative analysis of cells from *Pst* DC3000- and mock-treatment revealed a large subpopulation of cells from infected leaves comprising clusters M1 to M5 (Figure S1D and Figure S3A-B). More than 70% of cells in clusters M1-M5 were exposed to pathogen treatment, representing 34.8% of all cells. Further examination revealed that expression of genes induced by bacterial infection in these five clusters were generally higher than other clusters (Figure S3C). We refer to these five clusters, M1-M5, as pathogen-responsive clusters. These results indicate major differential shifts in the plant cell response after pathogen exposure.

To investigate the transcriptional reprogramming occurring in each pathogen-responsive cluster, we carried out Gene Ontology (GO) analyses. Clusters M1 and M2 exhibited enrichment of GO terms related to defense response to bacterium, immune response, and response to salicylic acid (SA) (Figure S3D). Clusters M4 and M5 were enriched in terms related to response to jasmonic acid and water transport (Figure S3D). These results suggest opposite transcriptional responses in clusters M1-M2 versus M4-5. To confirm this result, we calculated immune and susceptibility response scores based on gene expression modules for sets of genes either known to be expressed during immunity or disease, or significantly enriched in clusters M4 and M5 (Figure 2A, Table S2). Consistent with the GO analyses, clusters M1 and M2 displayed a higher immune response score, while M4 and M5 displayed a higher susceptibility response score (Figure 2A). Cluster M3 did not display a strong average response score (Figure 2A).

Next, we analyzed the expression of known genes involved in immunity and susceptibility to *Pst* DC3000 (Figure 2B). Expression of known plant immune-related genes *PATHOGENESIS-RELATED 1* (*PR1*), *PHYTOALEXIN DEFICIENT 4* (*PAD4*), *ENHANCED DISEASE SUSCEPTIBILITY 5* (*EDS5*) and *avrRpt2 induced gene1* (*AIG1*) was induced in clusters M1-M2 compared to non-responsive mesophyll cell clusters (other, M6-M14). In contrast, clusters M4-5 displayed induced expression of genes in susceptibility including those involved in jasmonic acid and abscisic acid (ABA) synthesis (e.g., *LIPOXYGENASE2* (*LOX2*) and *ABA DEFICIENT 1* (*ABA1*)). Specific transcripts related to both immunity and susceptibility were induced in cluster M3, but at lower magnitude compared to clusters M1-M2 and M4-M5 (Figure 2A and Figure S4). Cluster M2 exhibited the strongest activation of immune-related genes and related biological processes (Figure 2A-B and Figure S3D). These data indicate that M1-M2 represent immune activated clusters, M3 is a transition cluster, and M4-M5 represent susceptibility clusters (Figure 2A-B). *Pst* DC3000 is able to cause disease on *Arabidopsis* and consistent with a compatible interaction, M5 represents the largest cluster (14.2% of 11, 895 cells, Figure S1D).

Within a tissue, there are multiple points of infection representing different stages of disease development. Pseudotime analyses, which aim to order cells relative to a temporal, developmental or treatment axis, have been used to model the trajectory of a biological process, with each cell signifying a singular time point along a continuum (Trapnell et al., 2014). In order to predict the trajectory of pathogen-responsive cellular clusters, we performed pseudotime analysis using Monocle3 (Cao et al., 2019; Qiu et al., 2017b, 2017a; Trapnell et al., 2014). To circumvent influence of different cell types, we used *Pst* DC3000-treated mesophyll cells from clusters M1-M14 to infer the trajectory of disease progression. The trajectory was mostly linear, progressing through non-pathogen responsive clusters (M6-14), followed by immune clusters (M1-2), the transition cluster M3 and ended in the susceptible clusters (M4-M5, Figure 2C). In order to investigate pathogen responsiveness through pseudotime, a signature score was computed to quantify the overall impact *Pst* DC3000 has on each cell utilizing module scores from genes identified as differentially expressed in our bulk RNA-seq data. When overlaid upon pseudotime, the *Pst* DC3000 signature score was markedly induced in cells undergoing immunity (clusters M1-2), then plateaued or decreased through cells experiencing features associated with disease susceptibility (clusters M3-M5), consistent with the dynamic nature of plant-pathogen interactions (Figure 2D). These results indicate in a compatible interaction, disease progresses from plant defense, into a transitional state and culminates in susceptibility.

We also sought to identify genes that have dynamic expression patterns relative to the imputed pseudotime axis. Here, we again used monocle3 to identify genes that vary significantly with pseudotime, retrieving 776 loci (Figure S5 and Table S3). We clustered these into seven groups, with two clusters having expression profiles consistent with a

susceptibility response (clusters 2 and 6), while four clusters had profiles consistent with immunity or the transition between immunity and susceptibility (clusters 3-5 and 7) (Figure S5 and Table S3). Genes within clusters consistent with a susceptibility or immune response represent candidates important in disease progression (Figure S5). We also identified unique transcripts expressed in immunity, transition and susceptibility clusters (Figure S4).

Visualization of immune and susceptible cellular markers during disease progression

We sought to experimentally validate pseudotime predictions and investigate expression of immune and susceptible markers through the course of infection. We utilized surface inoculation, which more closely mimics natural infection, on two-week-old *Arabidopsis* seedlings. In order to test the experimental setup, we first monitored the growth of *Pst* DC3000-mCherry (Figure 3A). Bacterial titers did not change in the first 4h post-inoculation (hpi), but dramatically increased from 24-72hpi, consistent with previous experiments on seedlings and soil-grown plants (Figure 3A left) (Katagiri et al., 2002 and Ishiga et al., 2011). We visualized spatiotemporal dynamics of bacterial colonization after surface inoculation. At 24hpi, spotty fluorescence signals were observed (Figure 3A middle), which was similar to syringe-infiltration (Figure 1A). Visualizing multiple focal planes of bacterial fluorescence signals demonstrated that bacteria colonized intercellular space between mesophyll cells by 24hpi. At 48 and 72hpi, we observed enlarged and merged fluorescent spots, indicating high multiplication of bacterial populations at these stages (Figure 3A middle). Quantification of fluorescence intensity per colony showed a continuous increase over time (Figure 3A right).

We then visualized the expression patterns of cell cluster marker genes and fluorescently tagged *Pst* DC3000 during the course of infection. We selected marker genes that showed relatively high and specific expression from scRNA-seq analyses in either immune or susceptible clusters. Fluorescent transcriptional reporter lines coupled to a nuclear localization signal (NLS) enabled visualization of cell specific plant responses during pathogen infection.

Three immune marker genes were selected: *FLG22-INDUCED RECEPTOR-LIKE KINASE 1* (*FRK1*), *AT3G18250* (*LIPOPROTEIN 1, LipoP1*) and *CALMODULIN BINDING PROTEIN 60g* (*CBP60g*). *FRK1* is a receptor-like kinase that is strongly induced during pattern-triggered immunity and at early stages after pathogen infection (Asai et al., 2002; He et al., 2006). *LipoP1* is a putative membrane lipoprotein, whose function is unknown. The *CBP60g* transcription factor regulates biosynthesis of the plant defense hormone salicylic acid (Kim et al., 2022; Zhang et al., 2010). All three markers displayed high expression in immune clusters M1-2, variable expression in the transition cluster M3, but low expression in susceptible clusters M4-5 (Figure 3B-D left).

Using a previously characterized transcriptional reporter *pFRK1::NLS-3xmVENUS* (Zhou et al., 2020) and newly generated transgenic lines *pLipoP1/pCBP60g::NLS-3xmCitrine*, we observed low fluorescence signals in mock-inoculated *Arabidopsis* true leaves (Mock, Figure 3B-3D). *FRK1* expression was strongly induced at 24hpi and dramatically downregulated at 48 and 72hpi (Figure 3B). *FRK1* was previously shown to be strongly induced 2h post-syringe infiltration with *Pst* DC3000 using qPCR (He et al., 2006). These results suggest that the expression of *FRK1* at 24hpi represents an early infection stage using surface inoculation. We observed the expression of *LipoP1* and *CBP60g* was highly induced at 24-48hpi (Figure 3C and 3D). While *FRK1* and *LipoP1* exhibited more localized induction at 24hpi, *CBP60g* was more broadly expressed. The expression of all immune markers was significantly reduced at 72hpi when plants exhibited chlorosis and water-soaked symptoms (Figure 3B-D). A second independent transgenic line of *pLipoP1::NLS-3xmCitrine* exhibited a similar expression pattern, but had more robust expression at 72h (Figure S6A). A previous transcriptional reporter *CBP60gpro:EYFP-NLS* has been characterized and this line exhibited similar baseline expression as well as expression in skirt cells (see below, Matsumura et al., 2022). Together, these data highlight activation of immune marker genes at early infection stages and downregulation at late stages, consistent with the pseudotime trajectory.

We explored expression of three susceptibility marker genes strongly expressed in clusters M4-5: *EXPANSIN A10* (*EXPA10*), *PLASMA MEMBRANE INTRINSIC PROTEIN 1;4* (*PIP1;4*) and *IAA-leu-resistant-like5* (*ILL5*). *EXPA10* belongs to the expansin gene family whose members are able to induce cell wall loosening through a non-enzymatic function and have been implicated in plant-pathogen interactions (Cosgrove, 2015; Ding et al., 2008). *PIP1;4* is a plasma membrane localized aquaporin. Of the 13 *PIP* family members in *Arabidopsis*, 10 were significantly induced in clusters M4-M5. Aquaporins are membrane channels that facilitate the transport of water and small neutral molecules (H_2O, H_2O_2, CO_2) (Maurel et al., 2015). *ILL5* is most similar to *ILL3,* which encodes an amidohydrolase, involved in converting indole-3-acetic acid (IAA) from an amino acid conjugate to a free form to increase auxin signaling (Casanova-Sáez and Voß, 2019; Hayashi et al., 2021). All three markers displayed high expression in susceptibility clusters M4-5 (Figure 4A-C, left). *EXPA10* and *ILL5* had relatively weak expression in the transition cluster M3 and low expression in immune clusters M1-M2 (Figure 4A, 4C). In contrast, *PIP1;4* was expressed in clusters M1-M3, but at a lower level than M4-5 (Figure 4B).

We examined the expression of two independent transgenic lines for each susceptibility marker after inoculation with *Pst* DC3000 and observed similar results for both lines (*pEXPA10::NLS-3xmCitrine*, *pPIP1;4::NLS-3xmCitrine, pILL5::NLS-3xmCitrine,* Figure 4A-C, Figure S6B-D). The *EXPA10* and *PIP1;4* transcriptional reporter lines exhibited low levels of expression in mock-inoculated plants and increasing levels of expression after inoculation, peaking at 72hpi (Figure 4A-B, Figure S6B-C). The *ILL5* transcriptional

reporter lines exhibited low levels of expression in mock-inoculated plants and increasing levels of expression, peaking at 48hpi (Figure 4C, Figure S6D). *ILL5* expression decreased slightly at 72hpi, but was still higher than 24hpi (Figure 4C, Figure S6D). Thus, the susceptible markers are activated after bacterial infection and strongly induced during later infection stages. These data highlight expression of susceptibility genes at later infection stages, consistent with the pseudotime trajectory.

Immune and susceptible marker genes exhibit diverse patterns of spatial expression

Bacteria exhibit heterogeneity in colonization of a leaf after both syringe and surface inoculation (Figure 1A, Figure 3A). Our transcriptional reporter lines enabled us to probe marker gene expression with high sensitivity and at single-cell resolution. Therefore, we investigated where pathogen-responsive cells are spatially localized after surface inoculation with *Pst* DC3000. First, we examined expression of the *FRK1* immune marker gene at 24hpi when it showed highest expression (Figure 3B). *FRK1* was rarely expressed in mock samples, but was frequently observed in cells surrounding substomatal cavities colonized by bacteria (Figure 5A). *P. syringae* uses stomatal pores to enter the leaf interior and colonize the substomatal cavity early during infection (Melotto et al., 2008). We quantified confocal micrographs to determine the spatial localization of *FRK1* expressing cells. 91% of cells expressing *FRK1* after *Pst* DC3000 inoculation surrounded substomatal cavities (Figure 5B). Next, we quantified the proximity of *FRK1* expressing cells to bacterial colonies. 75% of *FRK1* expressing cells were proximal (< 15 µm) to bacterial colonies (Figure 5C). These data demonstrate that *FRK1*, which is known to be one of the earliest PTI marker genes, exhibits strong and specific expression at sites of bacterial invasion.

In contrast to *FRK1*, the *LipoP1* transcriptional reporter line exhibited dynamic changes in spatial expression patterns during the course of infection. *LipoP1* is expressed in guard cells, which flank stomatal pores, in the absence of pathogen infection (Figure 3C, Figure S6A). At 24hpi, 60% of *LipoP1* expressing cells were proximal to bacterial colonies (< 15 µm, Figure S6E). However, *LipoP1* exhibited variable spatial expression at 48 and 72hpi, either generally induced in all cells or highly induced in cells surrounding bacterial colonies, possibly due to unsynchronized bacterial infection within a leaf.

CPB60g encodes a master immune transcription factor that works in parallel with SARD1 to synthesize the plant defense hormone SA (Kim et al., 2022; Sun et al., 2015). In the absence of pathogen infection, *CBP60g* is expressed surrounding trichomes and in skirt cells at the base of trichomes (Figure 5D). These observations are consistent with those of Matsumara et al (2022), who observed a similar pattern of *CBP60g* expression after applying a mechanical force. The coverslip we applied during confocal imaging also induces mechanical stimulation. After *Pst* DC3000 inoculation, the number

of skirt cells expressing *CPB60g* did not change, but there was a general induction in mesophyll and epidermal cells (Figure 5D-E). The general induction of *CPB60g* may be reflective of its role in SA biogenesis and regulation via NPR1 receptors, which are critical for within-leaf and systemic immune responses.

The intriguing spatial association of immune marker expression and bacterial colonization prompted us investigate if expression of susceptibility markers were spatially associated with bacterial colonization. We observed more broad expression of susceptibility markers in leaves after 48hpi, which contrasts with the more specific expression of the immune markers *FRK1* and *LipoP1* at 24hpi. Transcriptional reporter lines for *EXPA10* and *PIP1;4* exhibited detectable expression in epidermal and mesophyll cells in the absence of pathogen infection (Figure 4, Figure S6B-C). In contrast, *ILL5* was mainly expressed in guard cells in leaves without bacterial infection, but strongly induced at 48-72hpi in epidermal, mesophyll and guard cells (Figure 5F-G). Collectively, the transcriptional reporter lines representing immune and susceptible markers reveal distinct patterns of spatial and temporal expression during disease progression.

DISCUSSION

Plants respond to pathogen infection in a heterogeneous manner. Here, we revealed heterogeneity of plant responses at single-cell resolution using scRNA-seq coupled with confocal imaging of transcriptional reporter lines. Individual plant cells at immune, susceptible or transition states highlighted the gradient of responses within an infected leaf. Immune markers exhibit diverse spatial and temporal expression patterns while susceptible markers exhibit more general and sustained expression patterns in response to virulent *Pst* DC3000 (Figure 6).

Our understanding of host-pathogen interactions is largely influenced by assays investigating whole tissue samples. However, even after uniform inoculation, pathogens exhibit uneven penetration into the leaf interior and variable colonization within a tissue, which should result in variable host responses. For example, spores from the fungal pathogen *Zymoseptoria tritici* are able to continuously germinate on wheat leaves and their hyphae penetrate stomata for up to 10 days, resulting in multiple asynchronized infection stages at any given time (Fantozzi et al., 2021; Fones et al., 2017; Haueisen et al., 2019). *P. syringae* also exhibits uneven distribution on bean leaf surfaces, forming aggregates at leaf veins, crevices, trichomes and occasionally stomata (Björklöf et al., 2000). Similarly, we were able to visualize uneven colonization patterns of *Pst* DC3000 after syringe and surface inoculation on *Arabidopsis* (Figure 1A and 3A). Our sc-RNAseq analyses were able to simultaneously identify cell clusters exhibiting opposing biological processes (immunity and susceptibility) at 24h post-inoculation, indicating asynchronous infection stages even early during infection (Figure 2).

Although *Pst* DC3000 is virulent on *Arabidopsis*, the pathogen can still induce damage and carries MAMPs that can be perceived by plant pattern recognition receptors (flagellin, elongation factor Tu and 3'OH fatty acid epitopes), resulting in localized immune activated cell clusters. Previous research has found purified MAMP treatment can initiate transcriptional responses within 5 min and *Pst* DC3000 infiltration within 2h (Bjornson et al., 2021; Lewis et al., 2015). The pseudotime trajectory of our scRNA-seq data placed the immunity cell clusters at an early stage of disease progression (Figure 2D). We identified two immune cell clusters (Figure 2), possibly due to waves of PTI transcriptional responses (Bjornson et al., 2021). Consistent with these observations, our immune transcriptional reporter lines were also highly expressed at early infection time points (Figure 3). *FRK1* is a well-known early marker gene of PTI (He et al., 2006; Lewis et al., 2015; Zhou et al., 2020). We found *FRK1* expression was activated in cells surrounding substomatal cavities colonized by *Pst* DC3000 (Figure 3B and 5A-C). *Pst* DC3000 uses stomatal pores to enter leaves and substomatal cavities are an early site of pathogen colonization (Melotto et al., 2008). Similarly, the immune marker *LipoP1* exhibited proximal expression to bacterial colonies early during infection (Figure 3C and Figure S6). The clustering of immune markers in cells surrounding bacteria may indicate that these bacterial colonies carry or create sufficient MAMPs/DAMPs to induce defense. In contrast, the immune marker *CBP60g* was broadly induced at all infection stages, consistent with its role in inducing SA synthesis whose accumulation is required for defense within a leaf as well as systemic immune responses (Figure 5D-E) (Kim et al., 2022; Sun et al., 2015).

Plant pathogens deliver effectors into host cells to dampen immune responses and promote susceptibility (Garcia-Ruiz et al., 2021; Toruño et al., 2016). The timing and number of cells targeted for effector delivery also varies, but can occur within 3h after bacterial infiltration on *Arabidopsis* (Grant et al., 2000; Henry et al., 2017). Transcriptional profiling of *Arabidopsis* infected by virulent *Pst* DC3000 detected effector-mediated suppression of PTI and upregulation of genes contributing to susceptibility by 6h (Lewis et al., 2015; Nobori et al., 2018). Our scRNA-seq and promoter reporter line investigations identified clusters of cells exhibiting patterns consistent with a compatible or susceptible interaction that peaked later during infection (Figure 2). Unlike the localized expression of *LipoP1* and *FRK1* immune markers, susceptibility markers exhibited more general expression, indicating more global reprogramming of the leaf to a susceptible state over time. The susceptibility markers *EXPA10* and *PIP1;4* encode members of gene families that function in cell wall enlargement/expansion and water transport under normal conditions, respectively (Cosgrove, 2015; Maurel et al., 2015). During infection these processes can be manipulated by pathogens to create favorable environments for proliferation and disease development (Ding et al., 2008; Xin et al., 2016).

Transcriptional profiling of entire tissues can mask cells at opposing response trajectories by averaging signals across thousands of cells. Comparing gene regulation in immune (M1-M2) and susceptible (M4-M5) clusters has resulted in the identification of novel candidates (Figure S4-S5 and Table S3), including specific members of large gene families, involved in foliar plant-pathogen interactions. Genes regulating plant immune perception and signaling have been well characterized over the past 30 years, but identification of susceptibility genes has lagged behind (van Schie and Takken, 2014). Susceptibility genes are attractive targets to modify for developing disease resistant crops due to advances in genome editing technologies and decreased regulatory oversight (Garcia-Ruiz et al., 2021; Zaidi et al., 2018). Future advancements in high-resolution spatial transcriptomics enabling profiling of both plant and pathogen tissues, will facilitate investigating gene expression in a positional context in complex tissues (Nobori et al., 2022; Saarenpää et al., 2022). Detailed characterization of cellular states throughout disease development will enable a comprehensive understanding of mechanisms regulating disease progression.

ACKNOWLEDGMENTS

We thank Dr. Niko Geldner (University of Lausanne, Switzerland) for providing *FRK1* transcriptional reporter seeds, Dr. Lei Lei (Lanzhou University, China) for bulk RNA extraction from leaves and Dr. Pamela Ronald for use of their confocal microscope. We also would like to thank all the members in Coaker Lab for helpful discussions and input on the project. This work was supported by the grants to G. C. from the NIH R35GM136402. S.L. was supported by the Independent research fund Denmark (grant number 7026-00053B). B.K. was supported by a USDA NIFA Award 2017-67030-25920. The sequencing was carried out at the UC Davis Genome Center DNA Technologies and Expression Analysis Core, supported by a NIH Shared Instrumentation Grant 1S10OD010786-01.

AUTHOR CONTRIBUTIONS

J.Z., S.L., B.C. and G.C designed the study. S.L. prepared samples for RNA-seq, B.C. analyzed sequencing data, J.Z. performed all microscopy and promoter-reporter analyses, A.T. and B.G. assisted with developing promoter-reporter lines. B.K. developed tagged *Pst* DC300. J.Z., S.L., B.K., B.C., and G.C. participated in the discussion and interpretation of results. J.Z, B.C., and G.C. wrote the manuscript. All authors reviewed and approved the manuscript.

DECLARATION OF INTERESTS

The authors declare no competing interests

FIGURE TITLES AND LEGENDS

Figure 1. Single-cell RNA-seq profiling of *Arabidopsis* infected with *Pseudomonas syringae*

(A) Confocal micrograph of an *Arabidopsis* leaf 24 hours post-infiltration (hpi) with mCherry-tagged *Pst* DC3000 Δ*hopQ1* (*Pst* DC3000). The image is a maximum projection from 21 confocal Z-stacks. Chlorophyll autofluorescence is shown in grey. Scale bar = 100 µm.

(B and C) *Pst* DC3000 colony number and area in infiltrated leaf tissue shown in (A). Boxplot shows median with minimum and maximum values indicated (n = 10 images from 4 plants).

(D) Overview of the scRNA-seq experiment. Four-week-old *Arabidopsis* Col-0 was infiltrated with *Pst* DC3000 or 10mM $MgCl_2$. Twenty-four hpi, protoplasts were prepared using the Tape-*Arabidopsis* Sandwich method. Cells were isolated on the 10x genomics Chromium chip and sequenced using the Illumina NovaSeq6000 platform.

(E and F) Single Cell Uniform Manifold Approximation and Projection (UMAP) plots from both *Pst* DC3000 and mock-treated samples, colored according to cluster identities (E) and cell types (F). M: mesophyll, B: bundle sheath, P: parenchyma and procambium, G: guard cells, C: companion cells.

See also Figure S1-2 and Table S1.

Figure 2. scRNA-seq reveals a continuum of disease progression from immune to susceptible responses within leaf tissue

(A) UMAP plot visualizing the magnitude of response to pathogen infection. Dashed line outlines the pathogen-responsive clusters (M1-5). Immune and susceptibility response scores were calculated as gene expression modules (Methods) based on the cell-specific expression of sets of genes either known to be expressed during acute immunity or disease, or were significantly enriched in clusters M4 and M5. Blue (negative values) indicates more immune-like, red (positive values) indicates more susceptible-like.

(B) Dot plot of the relative expression and percent of cells expressing known plant immunity or susceptibility genes across different mesophyll cell populations in the integrated scRNA-seq data at 24hpi with *Pst* DC3000. Other = clusters M6-14 (mesophyll), Immunity = clusters M1-M2, Transition = cluster M3, Susceptibility = clusters M4-5.

(C) Pseudotime trajectory through mesophyll cells shows directed transition from immunity (M1-2) to susceptibility (M4-5). Mesophyll cells in clusters M1-14 were re-embedded in low-dimensional space, then subjected to trajectory inference using the Monocle3 package (Methods). An initial cell was chosen as having the lowest DC3000-induced expression signature (D). Cells colored by their cluster membership, with green cells belonging to non-responsive mesophyll cells (Other), blue cells belonging to immune clusters, orange cells corresponding to the transition cluster, and red cells belonging to susceptibility clusters.

(D) DC3000-induction signature throughout pseudotime. Pseudotime values computed from the trajectory shown in (C). A DC3000-signature score was defined as the module score (Methods) for genes repressed by DC3000 from our bulk RNA-seq analysis, subtracted from the module scores for those genes that were induced. Cells are colored as in (C), based on their cluster membership.
See also Figure S3-5 and Table S2-4.

Figure 3. Temporal dynamics of immune marker expression during *Pseudomonas* infection

(A) Analysis of bacterial growth over three days post-flood inoculation. Two-week-old *Arabidopsis* seedlings grown on Murashige-Skoog plates were surface-inoculated with mCherry-tagged *Pst* DC3000 at concentration of 1 x 10^7 colony forming units/ml (CFU/ml). Left: Analyses of bacterial growth over time. Middle: Confocal micrograph of representative images of mock or *Pst* DC3000-inoculated *Arabidopsis* leaves over time. Chlorophyll autofluorescence is shown in blue. Right: Bacterial populations were determined by quantifying mean fluorescence intensity (FI, mean gray values) per colony. Boxplots show median with minimum and maximum values (n = 3 images from 3 plants). Different letters indicate statistically significant differences ($p < 0.0001$, ANOVA with Tukey test).
(B, C and D) The immune markers *FRK1* (B), *LipoP1* (C) and *CBP60g* (D) are highly expressed at early infection stages but downregulated at late stages. Promoter-reporter lines for each immune marker were generated with fusion to 3xfluorophore possessing a nuclear localization signal (NLS). Left: Feature plot of immune markers in pathogen-responsive clusters. Dashed line outlines Clusters M1-M3. Middle: Representative images of immune marker expression at different infection stages. Plants were inoculated as described in (A) and mock images are taken at 24h. Pictures are maximum projections from confocal Z stacks. Right: Mean florescence intensity per nucleus was calculated and boxplot shows median with minimum and maximum values (n = 6 images from 3 plants). Different letters indicate statistically significant differences ($p < 0.0001$, ANOVA with Tukey test). Scale bars: 50 µm. All experiments were repeated at least two times with similar results.
See also Figure S6.

Figure 4. Temporal dynamics of susceptible marker expression during *Pseudomonas* infection

(A, B and C) The susceptible markers *EXPA10* (A), *PIP1;4* (B) and *ILL5* (C) are highly induced at late infection stages. Promoter-reporter lines for each immune marker were generated with fusion to 3xfluorophore possessing a nuclear localization signal (NLS). Left: Feature plot of susceptible markers in pathogen-responsive clusters. Dashed line outlines clusters M4-M5. Middle: Representative images of susceptible marker expression at different infection stages. Two-week-old *Arabidopsis* seedlings grown on Murashige-Skoog plates were surface-inoculated with mCherry-tagged *Pst* DC3000 and mock images were taken at 24h. Pictures are maximum projections from confocal Z

stacks. Right: Mean florescence intensity (FI, mean gray values) per nucleus was calculated and boxplot shows median with minimum and maximum values indicated (n = 6 images from 3 plants). Different letters indicate statistically significant differences ($p < 0.0001$, ANOVA with Tukey test). All experiments were repeated at least two times with similar results. Scale bars: 50 µm.
See also Figure S6.

Figure 5. Spatial dynamics of immune and susceptible marker expression after *Pseudomonas* infection

(A-C) The immune marker *FRK1* is induced in surrounding cells of substomatal cavities colonized by *Pseudomonas syringae* DC3000. Two-week old *Arabidopsis pFRK1::NLS-3xmVENUS* seedlings were flood-inoculated with mCherry-tagged *Pst* DC3000. (A) At 24hpi, whole seedlings were fixed and cleared using ClearSee. Green asterisks indicate stomata. Left: A single image of bright field channel. Middle: Maximum projections of Z stack of mVENUS and mCherry signals. Right: Merged image. Scale bar: 20 µm.
(B) Percentage of *FRK1* expressing cells surrounding a substomatal cavity (+) or not (-) at 24hpi. Boxplot shows median with minimum and maximum values indicated (n = 7 images from 4 plants). ****$p < 0.0001$ analyzed by two-tailed, unpaired Student's t-test. The experiment was repeated twice with similar results.
(C) Percentage of *FRK1* expressing cells that are proximal (<15 µm) or distal (>15 µm) to a bacterial colony 24hpi. Data was analyzed as described in (B).
(D) The immune marker *CBP60g* is expressed in skirt cells at the trichome base before inoculation and broadly expressed after infection. *Arabidopsis pCBP60g::NLS-3xmCitrine* seedlings were inoculated as described in (A). Representative images of *CBP60g* expression at 24h in mock or DC3000-treated samples. Maximum projections of a Z stack of mCitrine signals were combined with a single image of chlorophyll autofluorescence. Chlorophyll autofluorescence is shown in blue. Red asterisks indicate skirt cells at the base of trichomes. Scale bars: 200 µm, and 50 µm in inset.
(E) Number of *CBP60g* expressing cells at 24h in mock- or DC3000-treated samples. Boxplot shows median with minimum and maximum values indicated (n = 10 images from 5 plants). $p < 0.0001$, ANOVA with Tukey test. The experiment was repeated twice with similar results.
(F) The susceptible marker *ILL5* is expressed in guard cells before inoculation and broadly expressed after infection. *Arabidopsis pILL5::NLS-3xmCitrine* seedlings were inoculated as described in (A). Representative images of *ILL5* expression at 48h in mock- or DC3000-treated samples. Maximum projections of Z stack of mCitrine signals were combined with single image of bright filed channel. Scale bar: 20 µm.
(G) Number of *ILL5* expressing cells at 24h in mock- or DC3000-treated samples. Boxplot shows median with minimum and maximum values indicated (n = 6 images from 3 plants). $p < 0.0001$, ANOVA with Tukey test. The experiment was repeated three times with similar results.
See also Figure S6.

Figure 6. Spatial and temporal model of immune and susceptible marker gene expression.

Immune and susceptible cell cluster markers exhibit diverse spatial and temporal expression patterns. Immune markers are highly induced at early infection stages, with *FRK1* and *LipoP1* induction in close proximity to bacterial colonies. At later time points (48h), the *FRK1* marker is no longer expressed, while other immune markers including *LipoP1* exhibit more general expression patterns throughout the leaf. Susceptible cell cluster markers exhibit basal expression that is broadly induced after infection throughout the leaf and peaks at late stages. Created with BioRender.com

STAR METHODS

RESOURCE AVAILABILITY

Lead contact

Further information and requests for resources and reagents should be directed to and will be fulfilled by the lead contact, Gitta Coaker (glcoaker@ucdavis.edu)

Materials availability

Seeds of transgenic plants generated in this study are deposited in *Arabidopsis* Biological Research Center (ABRC, stock number: CS73260 - CS73268). Plasmids used to generate transgenic plants are deposited in Addgene (192521-192525).

Data and code availability

scRNA-seq and bulk RNA-seq datasets generated in this study have been deposited at Gene Expression Omnibus (GSE213625) and are publicly available as of the date of publication. Code describing data analysis performed in this study are available as a github respository (https://www.github.com/b-coli/AtPst_SingleCell). Original microscopy images have been deposited in Zenodo (https://doi.org/10.5281/zenodo.7109010) and are publicly available as of the date of publication.

EXPERIMENTAL MODEL AND SUBJECT DETAILS

Plant material and growth conditions

Arabidopsis thaliana ecotype Columbia Col-0 was used in single-cell RNA sequencing, bacterial growth curves and plant transformation. The transcriptional reporter line *pFRK1::NLS-3xmVENUS* in the Col-0 background was obtained from Professor Niko Geldner's lab (Zhou et al., 2020).

Arabidopsis thaliana seeds (Col-0 or transgenic lines) were stratified for 2 days in the dark at 4°C before sowing onto soil or half-strength (1/2) Murashige and Skoog (MS) medium. Seeds were also surface-sterilized with disinfection solution (50% Bleach, 0.1% Tween-20) for 8 min and 75% ethanol for 1 min, washed thoroughly in sterile water for 4 times before sowing onto 1/2 MS medium. Four-week-old *A. thaliana* Col-0 used for scRNA-seq and plant transformation were grown in a controlled environment chamber at 22°C and 70% relative humidity with 10-h light/ 14-h dark photoperiod (100 μM m^{-2} s^{-1}). Ten to 14-day-old seedlings grown on 1/2 MS were incubated at 22°C under long-day conditions with 16-h light/ 8-h dark cycles. Seedlings were used for microscopy analyses.

Bacterial strains and growth conditions

Pseudomonas syringae pv. tomato DC3000 *ΔhopQ1* was labeled with 3xmCherry (*att*Tn*7*-3xmCherry, *Pst* DC3000-mCherry) using the same approach described previously (Baltrus et al., 2022). Bacteria were cultured overnight at 28°C on nutrient

yeast glycerol agar (NYGA) medium containing 100 µg/mL of rifampicin and 50 µg/mL of spectinomycin prior to inoculation.

METHOD DETAILS

Bacterial inoculation and quantification

Cells from an overnight culture of *Pst* DC3000-mCherry were collected and resuspended in 10mM $MgCl_2$. For scRNA-seq, bulk protoplast RNA-seq, and leaf RNA-seq samples, leaves of four-week-old *A. thaliana* were syringe infiltrated with a bacterial suspension of OD_{600} = 0.0001. Inoculated plants were kept under ambient humidity for 1 h to allow evaporation of excess water on the leaf surface. Then plants were covered with a transparent dome to maintain high humidity and incubated in growth chamber for 24h. For seedling flood inoculation, two-week-old plants on ½ MS medium were flood inoculated using 40 mL of the bacterial suspension of OD_{600} = 0.01 with 0.02% Silwet L-77 per 100 mm x 100 mm square petri dish (Fisherbrand). The bacterial suspension was removed after 20-30s incubation at room temperature. Inoculated plants were sealed with 3 M Micropore tape (3 M, St. Paul, MN, U.S.A.) and incubated in a growth chamber.

Bacterial titers after flood inoculation were determined as colony-forming units (CFU) per milligram at 0, 4, 24, 48, 72 hours post inoculation. In brief, three plants were cut roots away as one biological repeat, and 5-7 repeats were taken for each time. After measuring the weight of the aerial parts of each repeat, plants were ground and diluted in 5mM $MgCl_2$. The bacterial suspensions were then dilution plated on (NYGA) medium containing 100 µg/mL of rifampicin. Colonies were counted at each time point after incubation at 28°C.

Protoplast isolation

Protoplasts were isolated from *Arabidopsis* leaves infiltrated by bacteria and 10 mM $MgCl_2$ (Mock) using Tape-*Arabidopsis* Sandwich method as described previously (Wu et al., 2009). The adaxial side of 10-20 infiltrated leaves for each treatment was stabilized on the time tape and the abaxial side was adhered to the Magic tape (3M). The abaxial side was removed by carefully pulling off the Magic tape. Peeled leaves were immediately immersed in a petri dish containing 10 mL of enzyme solution (1.5% Cellulase Onuzuka R-10 (Yakult, Japan), 0.3% Macerozyme R-10, (Yakult, Japan), 0.4 M Mannitol, 20 mM KCl, 20 mM MES (2-(N-Morpholino)ethanesulfonic acid hydrate) pH 5.7, 10 mM CaCl2, and 0.1%, BSA). After digesting for 100 min with gentle shaking, the protoplast suspension was filtered through 40 µm cell strainer (BD Falcon 352340) into a round-bottomed 50 mL tube and centrifuged at 100 x g for 1 min at 22°C using a swinging rotor. Protoplast pellets were gently resuspended in 10 mL of CS-sucrose buffer (0.4 M sucrose, 20 mM MES pH 5.7, 20 mM KCl) and centrifuged at 100 x g for 2 min at 22°C. Intact and healthy protoplasts remained suspended in the upper layer. The upper layer suspension was then transferred into a clean round-bottomed tube and gently mixed with 10 mL of protoplast buffer (0.4 M Mannitol, 20 mM KCl, 20 mM MES

pH 5.7, and 0.1%, BSA). After centrifuging at 100x g for 2 min at 4°C using a swinging rotor, the supernatant was removed without disturbing the loosely packed protoplast pellets. The protoplast concentration was determined using a hemocytometer and the viability was checked using trypan blue solution. Two samples were prepared for each treatment.

scRNA-seq library preparation and sequencing

The protoplast suspension was diluted to a final concentration of 1000 cells/µL. A total of 40, 000 cells were loaded into a microfluidic chip (10X Genomics) with v3 chemistry to capture ~10,000 cells per sample. Protoplasts were barcoded with a Chromium Controller (10X Genomics). mRNA was reverse transcribed and cDNA libraries were constructed with a Chromium Single Cell 3' reagent kit V3 (10X Genomics) according to the manufacturer's instructions. Eleven cycles were used for cDNA amplification and 10 cycles were used for final library amplification. cDNA and final library quality was assessed using a Bioanalyzer 2100 High Sensitivity DNA Chip (Agilent). Sequencing of paired-end 150 bp reads was performed with a NovaSeq 6000 instrument (Illumina) at the University of California Davis Genome Center.

RNA extraction, bulk RNA-seq library preparation and sequencing

Total RNA was extracted with TRIzol (Fisher #15596018), following the manufacturer's instructions, for infiltrated leaves and leaf protoplasts isolated using the above mentioned method for scRNA-seq. DNase treatments were performed with RQ1 RNase-Free DNase (Promega #PR-M6101). Three biological replicates were performed for samples of *Pst* DC3000- or mock-infiltrated leaves, and one repeat was made for leaf protoplasts of each sample. cDNA libraries were prepared with QuantSeq FWD kit (Lexogen), according to the manufacturer's protocol. The fragment size distribution was evaluated by a Bioanalyzer 2100 (Agilent). The library pool was treated using Exonuclease VII (NEB), SPRI-bead purified with KapaPure beads (Kapa Biosystems /Roche), quantified via qPCR with a Kapa Library Quant kit (Kapa Biosystems) on a QuantStudio 5 RT-PCR system (Applied Biosystems). Sequencing was performed at the University of California Davis Genome Center using a HiSeq 4000 (Illumina) platform with single-end 100-bp reads.

Bulk RNA-seq data analysis

Raw fastq files for three bulk RNA-seq replicates each for *Pst* DC3000- and mock-inoculated leaves, as well as one bulk RNA-seq replicate from protoplasts isolated from *Pst* DC3000- and mock-inoculated leaves were trimmed using TrimGalore (stringency = 4, default parameters otherwise) and aligned to the *Arabidopsis thaliana* reference genome (Araport11) and quantified using STAR. Differential expression metrics for protoplasting and bacterial-induced changes were evaluated using the glmQLFit method from the edgeR package (Bioconductor v3.12). Genes determined to be significantly altered by protoplasting were those having log-fold change values > 0.5 and adjusted (BH) p-values less than 0.05. Genes determined to be significantly affected by *Pst*

DC3000 were those having log-fold change values >2 and adjusted (BH) p-values less than 0.01, unless otherwise specified.

scRNA-seq data initial processing and integration

Raw fastq files for the two samples generated in this study (Mock, *Pst* DC3000) were processed using Cellranger (v6.0.1; 10x Genomics, Pleasanton, CA) using default parameters (and an expected cell # equal to 10,000), mapping to the Araport11 *Arabidopsis* reference genome. The output from Cellranger was further processed using the Velocyto (v0.17.15) algorithm (La Manno et al., 2018), using default parameters, to generate spliced and unspliced counts matrices. For each cell, the percentage of reads mapping to mitochondrial, and chloroplast genes was computed. Cells were then filtered for those having a spliced mitochondrial read percentage of less than 1%, as well as a total spliced Unique Molecular Identifier (UMI) count within a dataset dependent threshold, bounded at the high end by 50,000 counts, and at the low end by 10% of the UMI count of the 100th most spliced transcript-rich cell for that dataset (Zheng et al., 2017).

Cells were normalized using the SCTransform method (Seurat, v3.9.9005). A recent *Arabidopsis* leaf single-cell RNA-seq dataset (Kim et al., 2021) was used to annotate cell types for all cells in this dataset using the label transfer pipeline (Seurat). Genes that were identified as being significantly influenced by protoplasting (see Bulk RNA-seq data analysis) were excluded from further analysis.

The *Pst* DC3000 and mock-inoculated datasets were then integrated using the anchor method (Seurat). Fifty principal components were calculated for the integrated dataset, used to cluster the cells (Louvain method, resolution 0.8) and further dimensionally reduce the gene expression space using Uniform Manifold Approximation and Projection (Seurat), using 50 Principal Components and default parameters (Table S1 and S6).

Pseudobulk analysis

A pseudobulk value for each gene was calculated as the sum of all counts from all cells for that gene within either the Mock- or *Pst* 3000-treated single-cell datasets. These values were then used to compare against whole-tissue or pooled-protoplast bulk RNA-seq data to verify that the single-cell datasets coarsely resemble bulk RNA-seq datasets.

Signature score computation

A *Pst* DC3000 signature score was computed as a composite metric quantifying the overall impact that *P. syringae* has on each cell. Here, the Seurat AddModuleScore function was used to define a pair of module score for genes up- or down-regulated by *Pst* DC3000 (from bulk RNA-seq data), with the signature score defined as the *Pst* DC3000-up module score subtracted from the *Pst* DC3000-down module score. Similarly, an Immunity Response Score was defined as a composite signature score

quantifying the general state that each cell was in with respect to disease progression based on sets of genes known to be induced/involved in immune response (Immunity) and in advanced disease (Susceptibility), supplemented with selected cluster marker loci from the scRNA-seq data (Table S2). Immune and Susceptibility module scores were computed using the AddModuleScore function (Seurat), and the Response Score was defined as the Susceptibility score subtracted from the Immunity score.

Cluster-specific marker loci

Marker genes specifically expressed in each cell cluster were determined using the FindAllMarkers function (Seurat) (Table S4). Significant markers were defined as those having a log-fold change (compared to all other clusters) greater than 0.25, and an adjusted (BH) p-value (wilcoxon rank sum test) less than 0.01. Log-fold change values between Mock- and *Pst* 3000-treated single-cell transcriptomes were computed for all superclusters (Immunity, Susceptibility, Transition, etc.) using the FindMarkers function (Seurat), with significance calculated using the DESeq2 (v1.30.1) method on the unnormalized counts.

GO Term Enrichment

For each cluster, a stringent set of marker loci was computed using the FindAllMarkers function in Seurat. GO term enrichment analysis was then performed using the topGO R package (Bioconductor version 3.12) for these marker genes, using all expressed genes (excluding those induced by protoplasting) as background. GO enrichment was calculated as the number of significant genes divided by the number of expected genes for each GO term.

Pseudotime inference

SCTransform-normalized expression values for spliced transcripts in mesophyll cells (excluding Seurat cluster 16, which seemed distinct from other mesophyll cells) were filtered from the *Pst* DC3000 dataset and re-embedded in a low-dimensional UMAP space using the Monocle3 (v1.0.0) pipeline (using 5 principal components, the correlation distance metric, and a minimum distance of 0.01). A cell trajectory was then imputed using Monocle3, defining the starting cell as that with the lowest *Pst* DC3000-expression score (a measure of how influenced the cell is by pathogen expression, empirically determined using bulk RNA-seq expression data) within the cluster with the lowest mean *Pst* DC3000 signature score, and a minimum branch length of 15. Pseudotime was projected onto this cell trajectory for *Pst* DC3000 mesophyll cells. Genes that vary significantly with pseudotime were computed with the graph_test function (Monocle3), using “principal graph” as the neighbor_graph parameter. Genes were selected as significant as those having a Morans I value greater than 0.2 (Table S3).

Generation of transgenic lines

Promoters (~ 2 kb upstream of the start codon) of *LipoP1* (AT3G18250, 2210 bp), *CBP60g* (AT5G26920, 2183 bp), *EXPA10* (AT1G26770, 2025 bp), *PIP1;4* (AT4G00430, 2151 bp) and *ILL5* (AT1G51780, 2089 bp) were PCR-amplified and fused to a nuclear localization signal (NLS) in pENTR vectors using In-Fusion HD Cloning Plus (Clontech). See Table S5 for primer details. The resulting constructs were recombined with binary destination vector pMpGWB123 (Ishizaki et al., 2015) bearing 3xmCitrine using Gateway Cloning Technology (Invitrogen). All plasmids were transformed into *Agrobacterium tumefaciens* GV3101 strain and then transformed into *A. thaliana* Col-0 by floral dipping method (Zhang et al., 2006). Seedlings of transgenic plants were screened on ½ MS plates supplemented with 25 µg/mL of hygromycin and 100 µg/mL of carbenicillin. Ten to fifteen independent T1 lines were analyzed for mCitrine fluorescence, and 3-5 T2 lines expressing mCitrine were selected for bacterial infection. Transgenic plants T2 or T3 (1-2 independent lines) with similar induction patterns after bacterial infection were selected for further experiments.

Confocal settings and image processing

Confocal imaging was performed on either a Leica TCS SP8 or Zeiss LSM 980 with Airyscan 2 laser scanning microscope. Pictures were taken with a 20x (Leica TCS SP8 or Zeiss LSM 980), 10x dry immersion objectives (Leica TCS SP8), as well as 5x immersion objective for tile-scan with 10% overlap (Leica TCS SP8). The following excitation and emission parameters were used for different fluorophores: mVENUS/mCitrine 488 nm, 493 – 540 nm; mCherry 552 nm, 586 – 635 nm; chlorophyll 638 nm, 650 -720 nm on Leica TCS SP8. mCitrine 488 nm, 490 – 543 nm; mCherry 561nm, 570 – 640 nm on Zeiss LSM 980. Sequential scanning was applied to avoid fluorescence interference between channels. Time-course confocal images of each transcriptional reporter line were taken under identical settings (lens, laser power, pinhole size, detector gain and interval of Z stack) for comparison of fluorescence intensity over time. Different microscope settings were applied for different transcriptional reporter lines according to the expression level of transgenes in plants.

Quantification of bacterial colony number, area, and fluorescence intensity was performed with the Imaris software (https://imaris.oxinst.com/). In brief, the Surface Model tool was used to quantify colony number and area of an entire image. Background subtraction was used to manually adjust threshold until all visible fluorescently-labeled bacteria colonies were detected. Then the detected colonies were counted and surface area measured. The Spot tool was used to build spots for each fluorescence domain to quantify fluorescence intensity. Quantification was determined by measurement of mean fluorescence intensity per spot (fluorescence intensity/nucleus). Algorithm settings of Different Spot Sizes were used due to variable nuclei size in different cell types of plant leaves. Background subtraction function was used for spot detection. To classify spots, “Quality (pixel intensity of a spot center)” filter was used to manually adjust threshold until all visible fluorescently-labeled nuclei were

detected. Spot regions were determined by manually adjusting threshold of absolute intensity detection to ensure complete coverage of fluorescently-labeled nuclei.

STATISTICAL ANALYSIS

Statistical analyses were performed with Graphpad Prism 9.0 software (https://www.graphpad.com/) or in R. The data are presented as mean ± SD, and “n” represents number of analyzed images from at least 3 plants. One-way ANOVA with Tukey’s test was used for multiple comparisons. Two tailed Student's t-test was used to compare means for two groups. Details about the statistical analyses are described in the figure legends.

SUPPLEMENTAL FIGURE TITLES AND LEGENDS

Figure S1. Summary statistics of single-cell datasets, and comparison with bulk RNA-seq. Related to Figure 1-2.

Transcript (A) and Gene (B) counts were summarized across all 11,895 cells in the integrated single-cell dataset. Median transcript counts were ~ 17,000 unique molecular identifier (UMI) per cell for both datasets, while median gene counts were ~ 3,500. (C) For Mock- and DC3000-treated single-cell datasets, a "pseudobulk" profile was calculated as the sum of counts per gene for all cells within that dataset. These profiles were compared to mRNA-seq data derived from whole leaves (Bulk Tissue) and pooled protoplasts (Protoplast) isolated in the same manner as those used for single-cell profiling). (D) Cell numbers from *Arabidopsis* leaves infiltrated with *Pst* DC3000 or 10mM $MgCl_2$ (Mock) in each cluster.

Figure S2. Integration of five leaf single-cell datasets from *Arabidopsis* preserves the unique identity of pathogen-treated cells. Related to Figure 1.

We integrated *Arabidopsis* leaf single-cell datasets (eight total, over five distinct studies: Kim et al., 2021; Liu et al., 2020; Lopez-Anido et al., 2021; Procko et al., 2022; Zhang et al., 2021) together to determine whether pathogen-treated cells remain distinct relative to other sources of cell-cell variation. (A) Cell type distribution in UMAP space for the integrated dataset. (B-H) Proportion of cells in UMAP space belonging to each individual dataset. While the combination of all datasets largely preserved clustering with respect to cell type (A), a region in UMAP space still appeared to be distinct for having *Pst* 3000-treated identity (C). Heatmap represents proportion of cells for each dataset overlaid onto the integrated UMAP.

Figure S3. Clusters M1 – M5 are pathogen-responsive clusters. Related to Figure 2.

(A) Single Cell Uniform Manifold Approximation and Projection (UMAP) plots from mock-treated samples (Mock) and *Pst* DC30000-treated samples, colored according to treatment. (B) Proportion of DC3000-treated cells is depicted in the UMAP of the combined single-cell RNA-seq datasets. These cells likely represent those that are responsive to pathogen infection. (C) A *Pst* DC3000 signature score was computed as a composite metric quantifying the overall impact that *P. syringae* has on each cell (Methods). The pathogen signature score is depicted in the UMAP of the combined scRNA-seq datasets. (D) GO-term enrichment (number of significant genes divided by the number of expected genes for each term) shows many terms specific to immunity and defense (bold, red) are associated with clusters M1-3, while terms specific to jasmonic acid, wounding and water stress (blue) are associated with clusters M4-5.

Figure S4. Overlap and specificity of differentially expressed genes in pathogen responsive clusters. Related to Figure 2.

Overlap among genes identified as differentially expressed among different pathogen-responsive mesophyll cell types in single-cell data (log2-fold change > 0.5, adjusted p-value < 0.01, and negative binomial test using DESeq2).

Figure S5. Variation of known and novel pathogen-responsive genes along pseudotime. Related to Figure 2 and Table S3.

(A) Expression is shown for genes known to be involved in pathogen responsiveness. Known genes are organized based on their suspected involvement in immunity (top) or in disease susceptibility (bottom) and expression in individual cells are depicted varying along pseudotime on the x-axis. (B) Novel clusters of genes exhibiting similar expression patterns that vary with pseudotime were identified using monocle3. Novel genes are organized based on a hierarchical clustering of scaled expression profiles over pseudotime. Y-axis represents individual genes within a cluster, and the X-axis represents expression in individual cells organized along pseudotime.

Figure S6. Visualization of immune and susceptible cellular markers during disease progression. Related to Figure 3-5.

Data represent experiments with a second, independent transgenic line for promoter-reporter constructs (line 2). (A) The immune marker *LipoP1* is highly expressed during infection. The promoter-reporter line for this immune marker was generated with fusion to 3xfluorophore possessing a nuclear localization signal (NLS). Two-week-old transgenic *Arabidopsis* seedlings grown on Murashige-Skoog plates were surface-inoculated with mCherry-tagged *Pst* DC3000 at concentration of 1 x 10^7 colony forming units/ml (CFU/ml). Left: Representative images of *LipoP1* expression at different infection stages. Mock images are taken at 24h. Pictures are maximum projections from confocal Z stacks. Right: Mean florescence intensity (FI, mean gray values) per nucleus was calculated and boxplot shows median with minimum and maximum values indicated (n = 6 images from 3 plants). Different letters indicate statistically significant differences ($p < 0.0001$, ANOVA with Tukey test). Scale bars: 50 µm. All experiments were repeated at least two times with similar results.

(B, C and D) The susceptible markers *EXPA10* (B), *PIP1;4* (C) and *ILL5* (D) are highly induced at late infection stages. Promoter-reporter lines for each susceptible marker were generated as mentioned in (A). Left: Representative images of susceptible marker expression at different infection stages. Plants were inoculated as described in (A) and mock images are taken at 24h. Pictures are maximum projections from confocal Z stacks. Right: Mean florescence intensity (mean gray values) per nucleus was calculated and boxplot shows median with minimum and maximum values indicated (n = 6 images from 3 plants). Different letters indicate statistically significant differences ($p < 0.0001$, one-way ANOVA with Tukey test). All experiments were repeated at least two times with similar results. Scale bars: 50 µm.

(E) Expression of *LipoP1* is proximal to bacterial colonies at 24hpi of *Pseudomonas* infection. Left: Confocal micrograph of representative images of *Pst* DC3000-inoculated

Arabidopsis leaves at 24hpi. Scale bars: 50 µm. Right: Percentage of *LipoP1* expressing cells that are proximal (<15 µm) or distal (>15 µm) to a bacterial colony 24hpi. Boxplot shows median with minimum and maximum values indicated (n = 6 images from 3 plants). ****$p < 0.0001$ analyzed by two-tailed, unpaired Student's t-test. Experiment was repeated three times with similar results.

SUPPLEMENTAL TABLE TITLES AND LEGENDS

Table S1. Cluster names and types. Related to Figure 1. Assignments of cell clusters identified by Seurat to broad cell types/states.

Table S2. Immunity and susceptibility genes used to calculate pathogen response score. Related to Figure 2 and STAR methods.

Table S3. Novel clusters of genes identified with pseudotime. Related to Figure 2 and S5. Scores, including spatial autocorrelation score (Moran's I), returned by Monocle3 for all genes in relation to Pseudotime. Genes with an associated module number (1-7) were identified as significantly correlated with Pseudotime.

Table S4. Marker genes in each cluster. Related to STAR methods. Per-gene marker statistics for all genes, determined by the FindAllMarkers function (Seurat). These describe the percentage of cells within (pct.1) and outside (pct.2) each cluster (seurat_clusters) that each gene is expressed, a p-value (p_val) for testing whether that gene is significantly enriched (Wilcox's rank sum test), an adjusted p-value (p_val_adj; using the Benjamini-Hochberg method).

Table S5. Primers used in this study. Related to STAR methods.

Table S6. Cell metadata information. Related to STAR methods. Per-cell metadata imputed for all cells in the integrated dataset. This includes transcript and gene counts for spliced, unspliced, and ambiguous mappings, number of transcripts derived from cholorplast (nCp) and mitochondrial (nMt) genes, the threshold UMI above which a cell was called from the raw counts matrix, the sample of origin (Sample_Name), statistics associated with SCT transformation, the predicted cell id and prediction scores for all cell types, a module score for pathogen responsiveness (DC3000.Up1 and DC3000.Down1), as well as cluster labels.

REFERENCES

Asai, T., Tena, G., Plotnikova, J., Willmann, M.R., Chiu, W.-L., Gomez-Gomez, L., Boller, T., Ausubel, F.M., and Sheen, J. (2002). MAP kinase signalling cascade in Arabidopsis innate immunity. Nature *415*, 977–983.

Alexa, A., & Rahnenfuhrer, J. (2021). topGO: Enrichment Analysis for Gene Ontology [Internet]. Bioconductor version: Release (3.12).

Berruyer, R., Poussier, S., Kankanala, P., Mosquera, G., and Valent, B. (2006). Quantitative and qualitative influence of inoculation methods on in planta growth of rice blast fungus. Phytopathology *96*, 346–355.

Björklöf, K., Nurmiaho-Lassila, E., Klinger, N., Haahtela, K., and Romantschuk, M. (2000). Colonization strategies and conjugal gene transfer of inoculated Pseudomonas syringae on the leaf surface. Journal of Applied Microbiology *89*, 423–432.

Bjornson, M., Pimprikar, P., Nürnberger, T., and Zipfel, C. (2021). The transcriptional landscape of Arabidopsis thaliana pattern-triggered immunity. Nature Plants *7*, 579–586.

Cao, J., Spielmann, M., Qiu, X., Huang, X., Ibrahim, D.M., Hill, A.J., Zhang, F., Mundlos, S., Christiansen, L., and Steemers, F.J. (2019). The single-cell transcriptional landscape of mammalian organogenesis. Nature *566*, 496–502.

Casanova-Sáez, R., and Voß, U. (2019). Auxin metabolism controls developmental decisions in land plants. Trends in Plant Science *24*, 741–754.

Cosgrove, D.J. (2015). Plant expansins: diversity and interactions with plant cell walls. Current Opinion in Plant Biology *25*, 162–172.

Cuppels, D.A. (1986). Generation and characterization of Tn 5 insertion mutations in Pseudomonas syringae pv. tomato. Applied and Environmental Microbiology *51*, 323–327.

Denyer, T., Ma, X., Klesen, S., Scacchi, E., Nieselt, K., and Timmermans, M.C.P. (2019). Spatiotemporal Developmental Trajectories in the Arabidopsis Root Revealed Using High-Throughput Single-Cell RNA Sequencing. Dev Cell *48*, 840-852 e5. https://doi.org/10.1016/j.devcel.2019.02.022.

Ding, X., Cao, Y., Huang, L., Zhao, J., Xu, C., Li, X., and Wang, S. (2008). Activation of the indole-3-acetic acid-amido synthetase GH3-8 suppresses expansin expression and promotes salicylate- and jasmonate-independent basal immunity in rice. Plant Cell *20*, 228–240. https://doi.org/10.1105/tpc.107.055657.

Fantozzi, E., Kilaru, S., Gurr, S.J., and Steinberg, G. (2021). Asynchronous development of Zymoseptoria tritici infection in wheat. Fungal Genetics and Biology *146*, 103504.

Fones, H.N., Eyles, C.J., Kay, W., Cowper, J., and Gurr, S.J. (2017). A role for random, humidity-dependent epiphytic growth prior to invasion of wheat by Zymoseptoria tritici. Fungal Genetics and Biology *106*, 51–60.

Garcia-Ruiz, H., Szurek, B., and Van den Ackerveken, G. (2021). Stop helping pathogens: engineering plant susceptibility genes for durable resistance. Current Opinion in Biotechnology *70*, 187–195.

Grant, M., Brown, I., Adams, S., Knight, M., Ainslie, A., and Mansfield, J. (2000). The RPM1 plant disease resistance gene facilitates a rapid and sustained increase in

cytosolic calcium that is necessary for the oxidative burst and hypersensitive cell death. The Plant Journal *23*, 441–450.
Hao, Y., Hao, S., Andersen-Nissen, E., Mauck III, W.M., Zheng, S., Butler, A., Lee, M.J., Wilk, A.J., Darby, C., and Zager, M. (2021). Integrated analysis of multimodal single-cell data. Cell *184*, 3573–3587.
Haueisen, J., Moller, M., Eschenbrenner, C.J., Grandaubert, J., Seybold, H., Adamiak, H., and Stukenbrock, E.H. (2019). Highly flexible infection programs in a specialized wheat pathogen. Ecol Evol *9*, 275–294. https://doi.org/10.1002/ece3.4724.
Hayashi, K.I., Arai, K., Aoi, Y., Tanaka, Y., Hira, H., Guo, R., Hu, Y., Ge, C., Zhao, Y., Kasahara, H., et al. (2021). The main oxidative inactivation pathway of the plant hormone auxin. Nat Commun *12*, 6752. https://doi.org/10.1038/s41467-021-27020-1.
He, P., Shan, L., Lin, N.-C., Martin, G.B., Kemmerling, B., Nürnberger, T., and Sheen, J. (2006). Specific bacterial suppressors of MAMP signaling upstream of MAPKKK in Arabidopsis innate immunity. Cell *125*, 563–575.
Henry, E., Toruño, T.Y., Jauneau, A., Deslandes, L., and Coaker, G. (2017). Direct and indirect visualization of bacterial effector delivery into diverse plant cell types during infection. The Plant Cell *29*, 1555–1570.
Ishizaki, K., Nishihama, R., Ueda, M., Inoue, K., Ishida, S., Nishimura, Y., Shikanai, T., and Kohchi, T. (2015). Development of Gateway Binary Vector Series with Four Different Selection Markers for the Liverwort Marchantia polymorpha. PLoS One *10*, e0138876. https://doi.org/10.1371/journal.pone.0138876.
Katagiri, F., Thilmony, R., and He, S.Y. (2002). The Arabidopsis thaliana-pseudomonas syringae interaction. Arabidopsis Book *1*, e0039. https://doi.org/10.1199/tab.0039.
Kim, J.H., Castroverde, C.D.M., Huang, S., Li, C., Hilleary, R., Seroka, A., Sohrabi, R., Medina-Yerena, D., Huot, B., and Wang, J. (2022). Increasing the resilience of plant immunity to a warming climate. Nature *607*, 339–344.
Kim, J.-Y., Symeonidi, E., Pang, T.Y., Denyer, T., Weidauer, D., Bezrutczyk, M., Miras, M., Zöllner, N., Hartwig, T., and Wudick, M.M. (2021). Distinct identities of leaf phloem cells revealed by single cell transcriptomics. The Plant Cell *33*, 511–530.
Kolodziejczyk, A.A., Kim, J.K., Svensson, V., Marioni, J.C., and Teichmann, S.A. (2015). The technology and biology of single-cell RNA sequencing. Molecular Cell *58*, 610–620.
La Manno, G., Soldatov, R., Zeisel, A., Braun, E., Hochgerner, H., Petukhov, V., Lidschreiber, K., Kastriti, M.E., Lönnerberg, P., and Furlan, A. (2018). RNA velocity of single cells. Nature *560*, 494–498.
Lewis, L.A., Polanski, K., de Torres-Zabala, M., Jayaraman, S., Bowden, L., Moore, J., Penfold, C.A., Jenkins, D.J., Hill, C., and Baxter, L. (2015). Transcriptional dynamics driving MAMP-triggered immunity and pathogen effector-mediated immunosuppression in Arabidopsis leaves following infection with Pseudomonas syringae pv tomato DC3000. The Plant Cell *27*, 3038–3064.
Libault, M., Pingault, L., Zogli, P., and Schiefelbein, J. (2017). Plant Systems Biology at the Single-Cell Level. Trends Plant Sci *22*, 949–960. https://doi.org/10.1016/j.tplants.2017.08.006.

Liu, Z., Zhou, Y., Guo, J., Li, J., Tian, Z., Zhu, Z., Wang, J., Wu, R., Zhang, B., and Hu, Y. (2020). Global dynamic molecular profiling of stomatal lineage cell development by single-cell RNA sequencing. Molecular Plant *13*, 1178–1193.

Liu, Z., Hou, S., Rodrigues, O., Wang, P., Luo, D., Munemasa, S., Lei, J., Liu, J., Ortiz-Morea, F.A., Wang, X., et al. (2022). Phytocytokine signalling reopens stomata in plant immunity and water loss. Nature *605*, 332–339. https://doi.org/10.1038/s41586-022-04684-3.

Lolle, S., Stevens, D., and Coaker, G. (2020). Plant NLR-triggered immunity: from receptor activation to downstream signaling. Curr Opin Immunol *62*, 99–105. https://doi.org/10.1016/j.coi.2019.12.007.

Lopez-Anido, C.B., Vatén, A., Smoot, N.K., Sharma, N., Guo, V., Gong, Y., Gil, M.X.A., Weimer, A.K., and Bergmann, D.C. (2021). Single-cell resolution of lineage trajectories in the Arabidopsis stomatal lineage and developing leaf. Developmental Cell *56*, 1043-1055. e4.

Macosko, E.Z., Basu, A., Satija, R., Nemesh, J., Shekhar, K., Goldman, M., Tirosh, I., Bialas, A.R., Kamitaki, N., and Martersteck, E.M. (2015). Highly parallel genome-wide expression profiling of individual cells using nanoliter droplets. Cell *161*, 1202–1214.

Matsumura, M., Nomoto, M., Itaya, T., Aratani, Y., Iwamoto, M., Matsuura, T., Hayashi, Y., Mori, T., Skelly, M.J., Yamamoto, Y.Y., et al. (2022). Mechanosensory trichome cells evoke a mechanical stimuli-induced immune response in Arabidopsis thaliana. Nat Commun *13*, 1216.

Matsumoto, A., Schlüter, T., Melkonian, K., Takeda, A., Nakagami, H., and Mine, A. (2022). A versatile Tn7 transposon-based bioluminescence tagging tool for quantitative and spatial detection of bacteria in plants. Plant Communications *3*, 100227.

Maurel, C., Boursiac, Y., Luu, D.-T., Santoni, V., Shahzad, Z., and Verdoucq, L. (2015). Aquaporins in plants. Physiological Reviews *95*, 1321–1358.

McCarthy, D.J., Chen, Y., and Smyth, G.K. (2012). Differential expression analysis of multifactor RNA-Seq experiments with respect to biological variation. Nucleic Acids Research *40*, 4288–4297.

Melotto, M., Underwood, W., and He, S.Y. (2008). Role of stomata in plant innate immunity and foliar bacterial diseases. Annual Review of Phytopathology *46*, 101. .

Nobori, T., Velásquez, A.C., Wu, J., Kvitko, B.H., Kremer, J.M., Wang, Y., He, S.Y., and Tsuda, K. (2018). Transcriptome landscape of a bacterial pathogen under plant immunity. Proceedings of the National Academy of Sciences *115*, E3055–E3064.

Nobori, T., Oliva, M., Lister, R., and Ecker, J.R. (2022). PHYTOMap: Multiplexed single-cell 3D spatial gene expression analysis in plant tissue. bioRxiv. https://doi.org/10.1101/2022.07.28.501915.

Pétriacq, P., Stassen, J.H., and Ton, J. (2016). Spore density determines infection strategy by the plant pathogenic fungus Plectosphaerella cucumerina. Plant Physiology *170*, 2325–2339.

Procko, C., Lee, T., Borsuk, A., Bargmann, B.O., Dabi, T., Nery, J.R., Estelle, M., Baird, L., O'Connor, C., and Brodersen, C. (2022). Leaf cell-specific and single-cell

transcriptional profiling reveals a role for the palisade layer in UV light protection. The Plant Cell.
Qiu, X., Hill, A., Packer, J., Lin, D., Ma, Y.-A., and Trapnell, C. (2017a). Single-cell mRNA quantification and differential analysis with Census. Nature Methods *14*, 309–315.
Qiu, X., Mao, Q., Tang, Y., Wang, L., Chawla, R., Pliner, H.A., and Trapnell, C. (2017b). Reversed graph embedding resolves complex single-cell trajectories. Nature Methods *14*, 979–982.
R Core Team (2019). R: a language and environment for statistical computing. R Foundation for Statistical Computing. https://www.R-project.org/
Robinson, M.D., McCarthy, D.J., and Smyth, G.K. (2010). edgeR: a Bioconductor package for differential expression analysis of digital gene expression data. Bioinformatics *26*, 139–140.
RStudio Team. (2019). RStudio: integrated devlopment for R. https://rstudio.com/products/rstudio/download/
Saarenpää, S., Shalev, O., Ashkenazy, H., de Oliveira-Carlos, V., Lundberg, D.S., Weigel, D., and Giacomello, S. (2022). Spatially resolved host-bacteria-fungi interactomes via spatial metatranscriptomics. bioRxiv. https://doi.org/10.1101/2022.07.18.496977.
van Schie, C.C., and Takken, F.L. (2014). Susceptibility genes 101: how to be a good host. Annual Review of Phytopathology *52*, 551–581.
Seyfferth, C., Renema, J., Wendrich, J.R., Eekhout, T., Seurinck, R., Vandamme, N., Blob, B., Saeys, Y., Helariutta, Y., Birnbaum, K.D., et al. (2021). Advances and Opportunities in Single-Cell Transcriptomics for Plant Research. Annu Rev Plant Biol *72*, 847–866. https://doi.org/10.1146/annurev-arplant-081720-010120.
Shahan, R., Hsu, C.-W., Nolan, T.M., Cole, B.J., Taylor, I.W., Greenstreet, L., Zhang, S., Afanassiev, A., Vlot, A.H.C., and Schiebinger, G. (2022). A single-cell Arabidopsis root atlas reveals developmental trajectories in wild-type and cell identity mutants. Developmental Cell *57*, 543-560. e9.
Sun, T., Zhang, Y., Li, Y., Zhang, Q., Ding, Y., and Zhang, Y. (2015). ChIP-seq reveals broad roles of SARD1 and CBP60g in regulating plant immunity. Nature Communications *6*, 1–12.
Tang, F., Barbacioru, C., Wang, Y., Nordman, E., Lee, C., Xu, N., Wang, X., Bodeau, J., Tuch, B.B., Siddiqui, A., et al. (2009). mRNA-Seq whole-transcriptome analysis of a single cell. Nat Methods *6*, 377–382. https://doi.org/10.1038/nmeth.1315.
Toruño, T.Y., Stergiopoulos, I., and Coaker, G. (2016). Plant-pathogen effectors: cellular probes interfering with plant defenses in spatial and temporal manners. Annual Review of Phytopathology *54*, 419.
Trapnell, C., Cacchiarelli, D., Grimsby, J., Pokharel, P., Li, S., Morse, M., Lennon, N.J., Livak, K.J., Mikkelsen, T.S., and Rinn, J.L. (2014). The dynamics and regulators of cell fate decisions are revealed by pseudotemporal ordering of single cells. Nature Biotechnology *32*, 381–386.
Wei, C., Kvitko, B.H., Shimizu, R., Crabill, E., Alfano, J.R., Lin, N., Martin, G.B., Huang, H., and Collmer, A. (2007). A Pseudomonas syringae pv. tomato DC3000 mutant lacking the type III effector HopQ1-1 is able to cause disease in the model plant Nicotiana benthamiana. The Plant Journal *51*, 32–46.

Whalen, M.C., Innes, R.W., Bent, A.F., and Staskawicz, B.J. (1991). Identification of Pseudomonas syringae pathogens of Arabidopsis and a bacterial locus determining avirulence on both Arabidopsis and soybean. The Plant Cell *3*, 49–59.

Wu, F.-H., Shen, S.-C., Lee, L.-Y., Lee, S.-H., Chan, M.-T., and Lin, C.-S. (2009). Tape-Arabidopsis Sandwich-a simpler Arabidopsis protoplast isolation method. Plant Methods *5*, 1–10.

Xin, X.F., Nomura, K., Aung, K., Velasquez, A.C., Yao, J., Boutrot, F., Chang, J.H., Zipfel, C., and He, S.Y. (2016). Bacteria establish an aqueous living space in plants crucial for virulence. Nature *539*, 524–529. https://doi.org/10.1038/nature20166.

Xin, X.-F., Kvitko, B., and He, S.Y. (2018). Pseudomonas syringae: what it takes to be a pathogen. Nature Reviews Microbiology *16*, 316–328.

Yuan, M., Ngou, B.P.M., Ding, P., and Xin, X.-F. (2021). PTI-ETI crosstalk: an integrative view of plant immunity. Current Opinion in Plant Biology *62*, 102030.

Zaidi, S.S.-A., Mukhtar, M.S., and Mansoor, S. (2018). Genome editing: targeting susceptibility genes for plant disease resistance. Trends in Biotechnology *36*, 898–906.

Zhang, T.Q., Xu, Z.G., Shang, G.D., and Wang, J.W. (2019). A Single-Cell RNA Sequencing Profiles the Developmental Landscape of Arabidopsis Root. Mol Plant *12*, 648–660. https://doi.org/10.1016/j.molp.2019.04.004.

Zhang, T.-Q., Chen, Y., and Wang, J.-W. (2021). A single-cell analysis of the Arabidopsis vegetative shoot apex. Developmental Cell *56*, 1056-1074. e8.

Zhang, X., Henriques, R., Lin, S.-S., Niu, Q.-W., and Chua, N.-H. (2006). Agrobacterium-mediated transformation of Arabidopsis thaliana using the floral dip method. Nature Protocols *1*, 641–646.

Zhang, Y., Xu, S., Ding, P., Wang, D., Cheng, Y.T., He, J., Gao, M., Xu, F., Li, Y., and Zhu, Z. (2010). Control of salicylic acid synthesis and systemic acquired resistance by two members of a plant-specific family of transcription factors. Proceedings of the National Academy of Sciences *107*, 18220–18225.

Zheng, G.X., Terry, J.M., Belgrader, P., Ryvkin, P., Bent, Z.W., Wilson, R., Ziraldo, S.B., Wheeler, T.D., McDermott, G.P., and Zhu, J. (2017). Massively parallel digital transcriptional profiling of single cells. Nature Communications *8*, 1–12.

Zhou, J.M., and Zhang, Y. (2020). Plant Immunity: Danger Perception and Signaling. Cell *181*, 978–989. https://doi.org/10.1016/j.cell.2020.04.028.

Zhou, F., Emonet, A., Denervaud Tendon, V., Marhavy, P., Wu, D., Lahaye, T., and Geldner, N. (2020). Co-incidence of Damage and Microbial Patterns Controls Localized Immune Responses in Roots. Cell *180*, 440-453 e18. https://doi.org/10.1016/j.cell.2020.01.013.

Zipfel, C., Kunze, G., Chinchilla, D., Caniard, A., Jones, J.D., Boller, T., and Felix, G. (2006). Perception of the bacterial PAMP EF-Tu by the receptor EFR restricts Agrobacterium-mediated transformation. Cell *125*, 749–760. https://doi.org/10.1016/j.cell.2006.03.037.

Figure 1

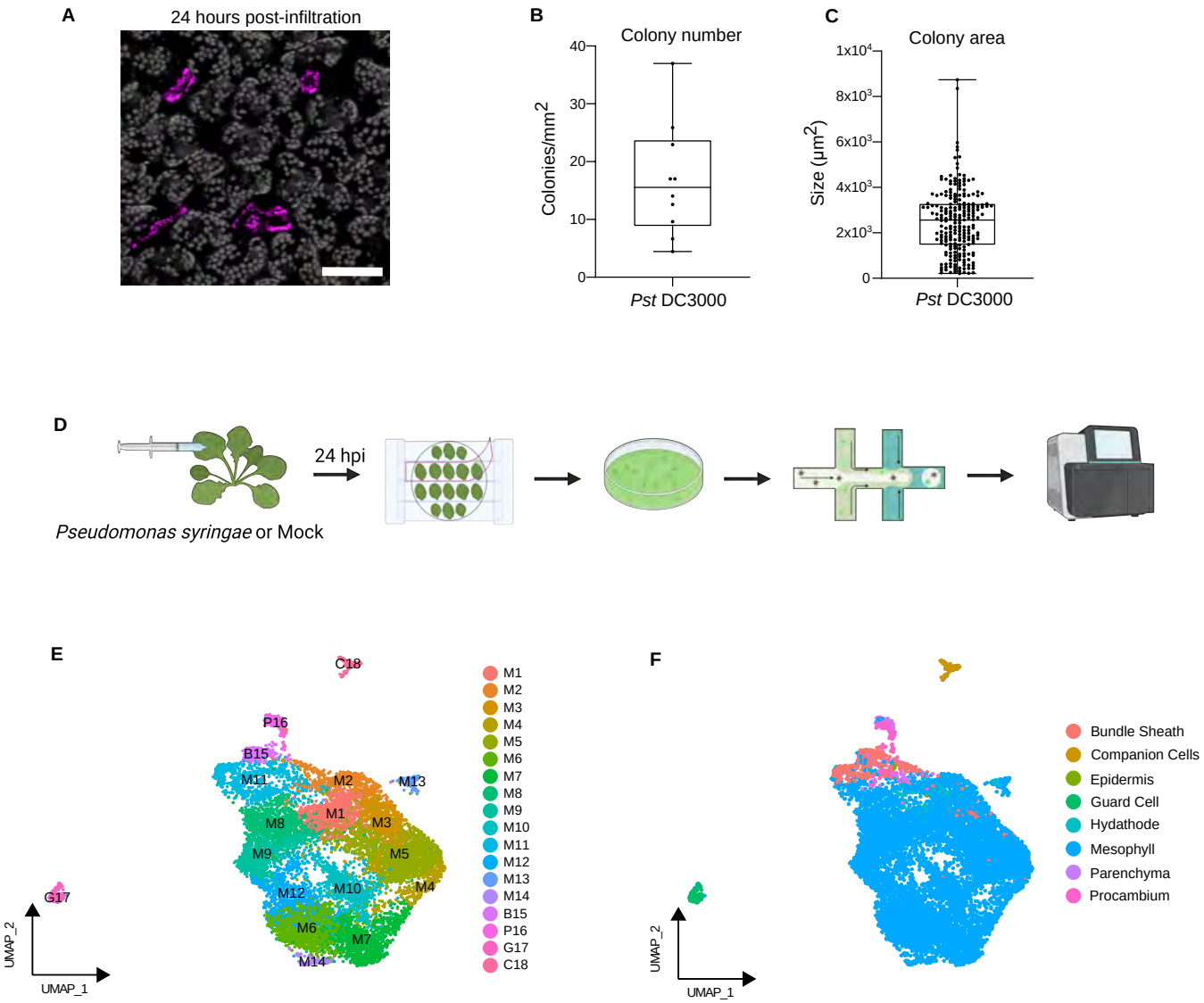

Figure 1. Single-cell RNA-seq profiling of *Arabidopsis* infected with *Pseudomonas syringae*

(A) Confocal micrograph of an *Arabidopsis* leaf 24 hours post-infiltration (hpi) with mCherry-tagged *Pst* DC3000 Δ*hopQ1* (*Pst* DC3000). The image is a maximum projection from 21 confocal Z-stacks. Chlorophyll autofluorescence is shown in grey. Scale bar = 100 µm.

(B and C) *Pst* DC3000 colony number and area in infiltrated leaf tissue shown in (A). Boxplot shows median with minimum and maximum values indicated (n = 10 images from 4 plants).

(D) Overview of the scRNA-seq experiment. Four-week-old *Arabidopsis* Col-0 was infiltrated with *Pst* DC3000 or 10mM $MgCl_2$. Twenty-four hpi, protoplasts were prepared using the Tape-*Arabidopsis* Sandwich method. Cells were isolated on the 10x genomics Chromium chip and sequenced using the Illumina NovaSeq6000 platform.

(E and F) Single Cell Uniform Manifold Approximation and Projection (UMAP) plots from both *Pst* DC3000 and mock-treated samples, colored according to cluster identities (E) and cell types (F). M: mesophyll, B: bundle sheath, P: parenchyma and procambium, G: guard cells, C: companion cells.

Figure 2

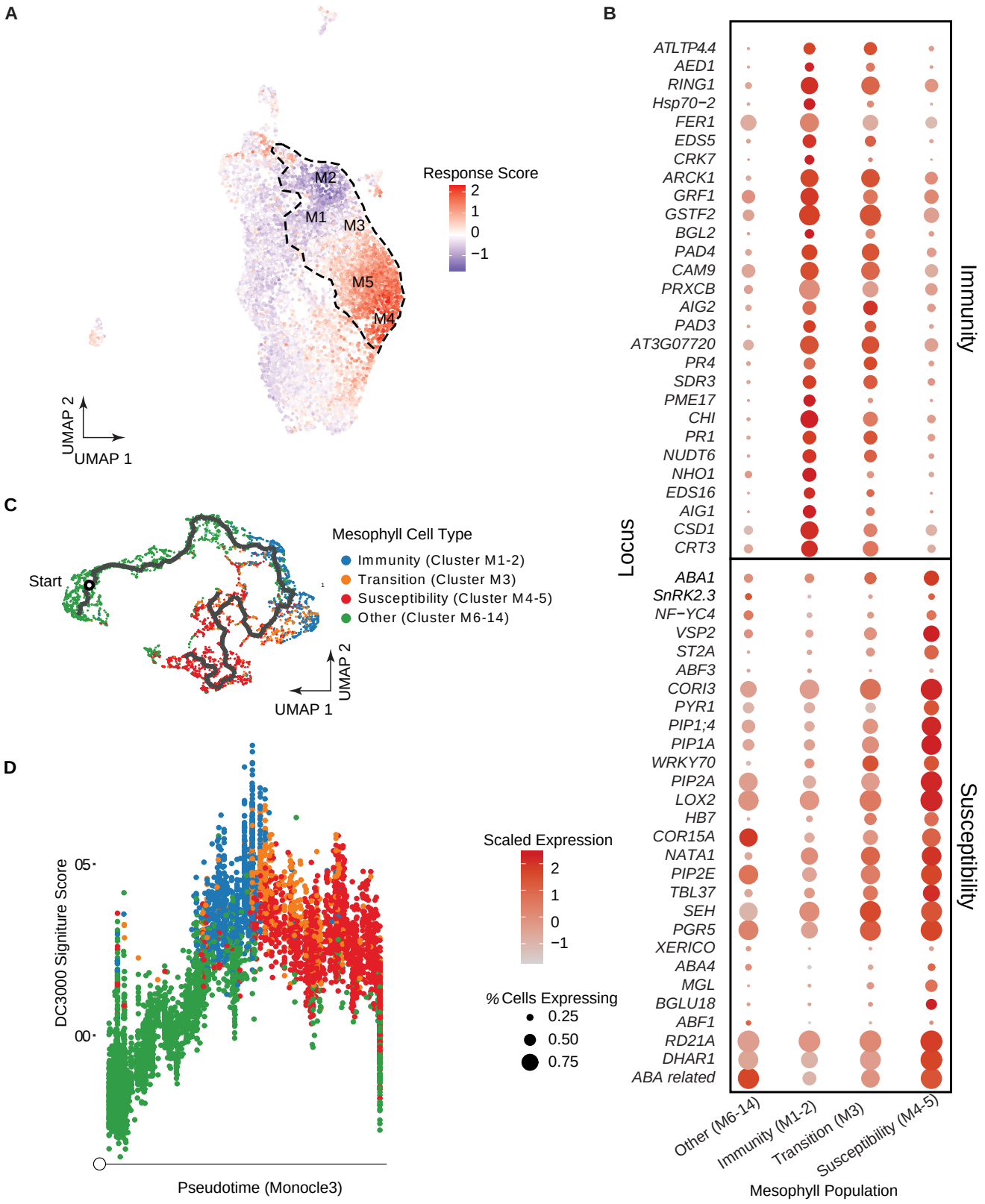
A
M2
M1
M3
M5
M4
Response Score
2
1
0
−1
UMAP 2
UMAP 1
C
Start
Mesophyll Cell Type
Immunity (Cluster M1-2)
Transition (Cluster M3)
Susceptibility (Cluster M4-5)
Other (Cluster M6-14)
UMAP 2
UMAP 1
D
DC3000 Signiture Score
Pseudotime (Monocle3)
Scaled Expression
2
1
0
−1
% Cells Expressing
0.25
0.50
0.75
B
ATLTP4.4
AED1
RING1
Hsp70−2
FER1
EDS5
CRK7
ARCK1
GRF1
GSTF2
BGL2
PAD4
CAM9
PRXCB
AIG2
PAD3
AT3G07720
PR4
SDR3
PME17
CHI
PR1
NUDT6
NHO1
EDS16
AIG1
CSD1
CRT3
ABA1
SnRK2.3
NF−YC4
VSP2
ST2A
ABF3
CORI3
PYR1
PIP1;4
PIP1A
WRKY70
PIP2A
LOX2
HB7
COR15A
NATA1
PIP2E
TBL37
SEH
PGR5
XERICO
ABA4
MGL
BGLU18
ABF1
RD21A
DHAR1
ABA related
Locus
Immunity
Susceptibility
Other (M6-14)
Immunity (M1-2)
Transition (M3)
Susceptibility (M4-5)
Mesophyll Population

Figure 2. scRNA-seq reveals a continuum of disease progression from immune to susceptible responses within leaf tissue

(A) UMAP plot visualizing the magnitude of response to pathogen infection. Dashed line outlines the pathogen-responsive clusters (M1-5). Immune and susceptibility response scores were calculated as gene expression modules (Methods) based on the cell-specific expression of sets of genes either known to be expressed during acute immunity or disease, or were significantly enriched in clusters M4 and M5. Blue (negative values) indicates more immune-like, red (positive values) indicates more susceptible-like.

(B) Dot plot of the relative expression and percent of cells expressing known plant immunity or susceptibility genes across different mesophyll cell populations in the integrated scRNA-seq data at 24hpi with *Pst* DC3000. Other = clusters M6-14 (mesophyll), Immunity = clusters M1-M2, Transition = cluster M3, Susceptibility = clusters M4-5.

(C) Pseudotime trajectory through mesophyll cells shows directed transition from immunity (M1-2) to susceptibility (M4-5). Mesophyll cells in clusters M1-14 were re-embedded in low-dimensional space, then subjected to trajectory inference using the Monocle3 package (Methods). An initial cell was chosen as having the lowest DC3000-induced expression signature (D). Cells colored by their cluster membership, with green cells belonging to non-responsive mesophyll cells (Other), blue cells belonging to immune clusters, orange cells corresponding to the transition cluster and red cells belonging to susceptibility clusters.

(D) DC3000-induction signature throughout pseudotime. Pseudotime values computed from the trajectory shown in (C). A DC3000-signature score was defined as the module score (Methods) for genes repressed by DC3000 from our bulk RNA-seq analysis, subtracted from the module scores for those genes that were induced. Cells are colored as in (C), based on their cluster membership.

Figure 3

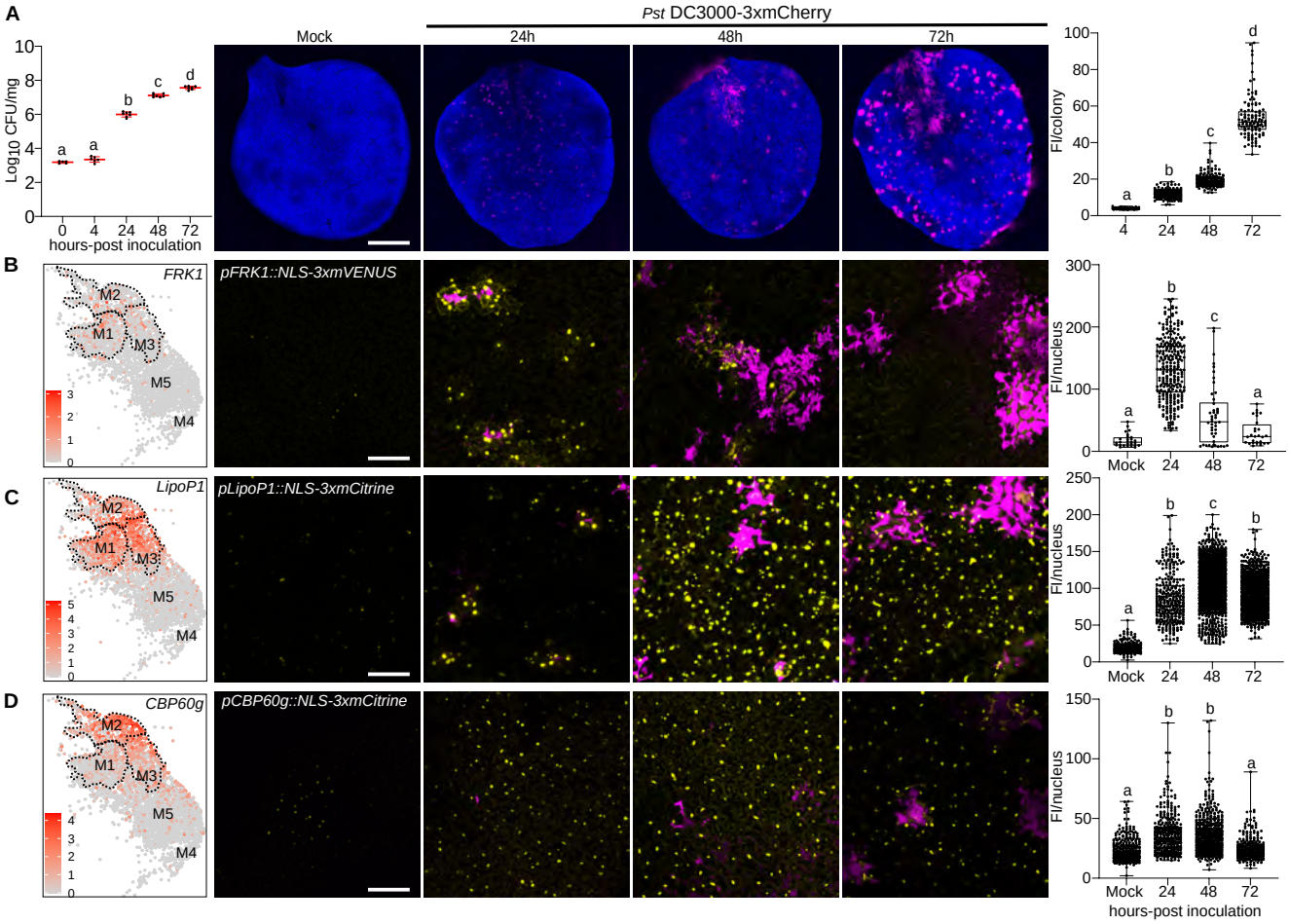

Figure 3. Temporal dynamics of immune marker expression during *Pseudomonas* infection

(A) Analysis of bacterial growth over three days post-flood inoculation. Two-week-old *Arabidopsis* seedlings grown on Murashige-Skoog plates were surface-inoculated with mCherry-tagged *Pst* DC3000 at concentration of 1 x 10^7 colony forming units/ml (CFU/ml). Left: Analyses of bacterial growth over time. Middle: Confocal micrograph of representative images of mock or *Pst* DC3000-inoculated *Arabidopsis* leaves over time. Chlorophyll autofluorescence is shown in blue. Right: Bacterial populations were determined by quantifying mean fluorescence intensity (FI, mean gray values) per colony. Boxplots show median with minimum and maximum values (n = 3 images from 3 plants). Different letters indicate statistically significant differences ($p < 0.0001$, ANOVA with Tukey test).

(B, C and D) The immune markers *FRK1* (B), *LipoP1* (C) and *CBP60g* (D) are highly expressed at early infection stages but downregulated at late stages. Promoter-reporter lines for each immune marker were generated with fusion to 3xfluorophore possessing a nuclear localization signal (NLS). Left: Feature plot of immune markers in pathogen-responsive clusters. Dashed line outlines Clusters M1-M3. Middle: Representative images of immune marker expression at different infection stages. Plants were inoculated as described in (A) and mock images are taken at 24h. Pictures are maximum projections from confocal Z stacks. Right: Mean florescence intensity per nucleus was calculated and boxplot shows median with minimum and maximum values (n = 6 images from 3 plants). Different letters indicate statistically significant differences ($p < 0.0001$, ANOVA with Tukey test). Scale bars: 50 µm. All experiments were repeated at least two times with similar results.

Figure 4

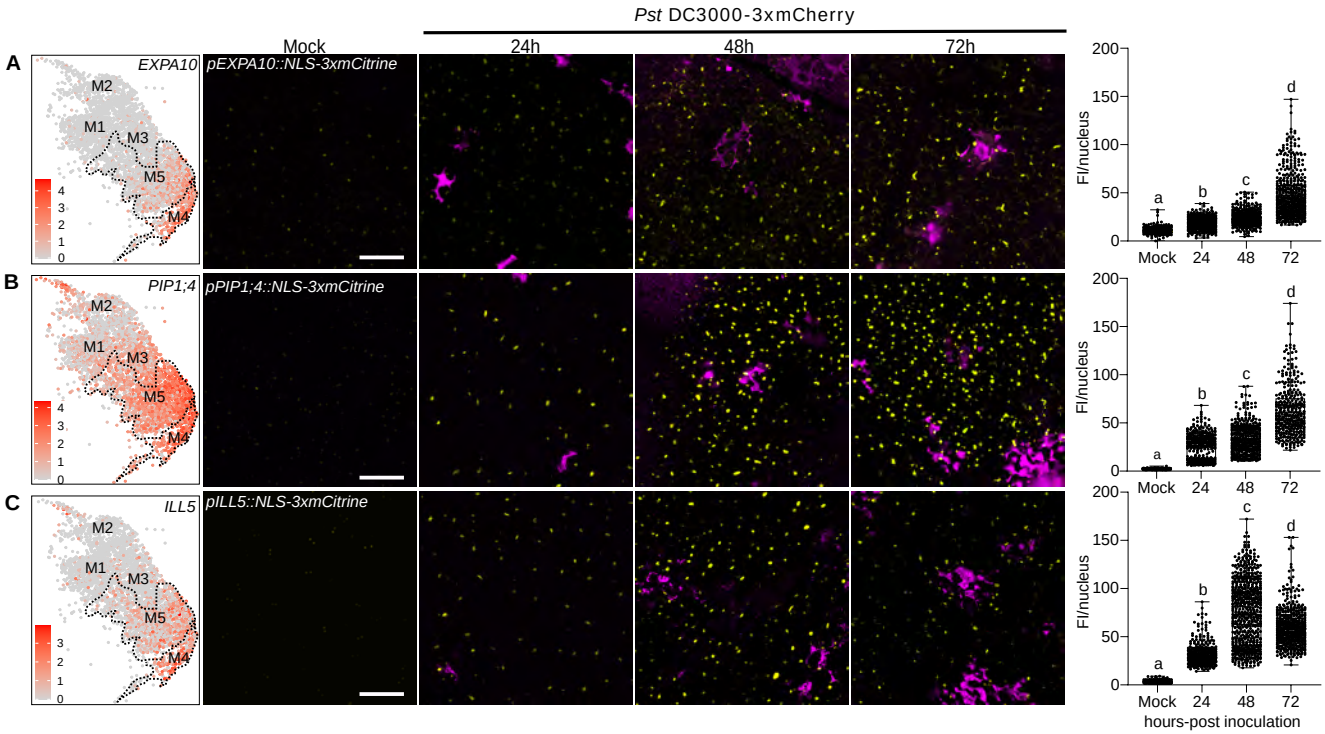

Figure 4. Temporal dynamics of susceptible marker expression during *Pseudomonas* infection

(A, B and C) The susceptible markers *EXPA10* (A), *PIP1;4* (B) and *ILL5* (C) are highly induced at late infection stages. Promoter-reporter lines for each immune marker were generated with fusion to 3xfluorophore possessing a nuclear localization signal (NLS). Left: Feature plot of susceptible markers in pathogen-responsive clusters. Dashed line outlines clusters M4-M5. Middle: Representative images of susceptible marker expression at different infection stages. Two-week-old *Arabidopsis* seedlings grown on Murashige-Skoog plates were surface-inoculated with mCherry-tagged *Pst* DC3000 and mock images were taken at 24h. Pictures are maximum projections from confocal Z stacks. Right: Mean florescence intensity (FI, mean gray values) per nucleus was calculated and boxplot shows median with minimum and maximum values indicated (n = 6 images from 3 plants). Different letters indicate statistically significant differences ($p < 0.0001$, ANOVA with Tukey test). All experiments were repeated at least two times with similar results. Scale bars: 50 µm.

Figure 5

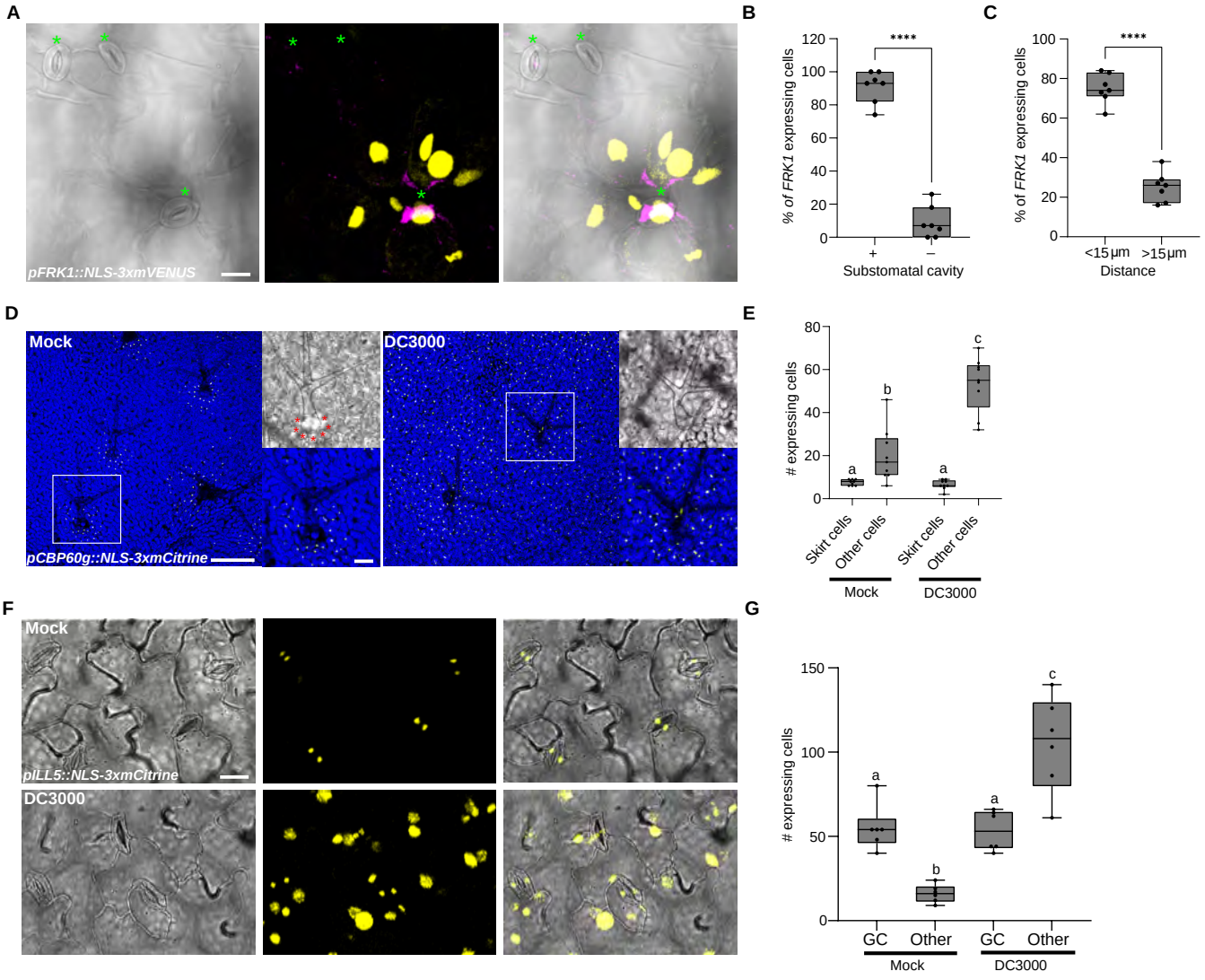
A
pFRK1::NLS-3xmVENUS
B
% of FRK1 expressing cells
****
+
−
Substomatal cavity
C
% of FRK1 expressing cells
****
<15 µm
>15 µm
Distance
D
Mock
DC3000
pCBP60g::NLS-3xmCitrine
E
expressing cells
Skirt cells
Other cells
Mock
DC3000
F
Mock
pILL5::NLS-3xmCitrine
DC3000
G
expressing cells
GC
Other
Mock
DC3000

Figure 5. Spatial dynamics of immune and susceptible marker expression after *Pseudomonas* infection

(A-C) The immune marker *FRK1* is induced in surrounding cells of substomatal cavities colonized by *Pseudomonas syringae* DC3000. Two-week old *Arabidopsis pFRK1::NLS-3xmVENUS* seedlings were flood-inoculated with mCherry-tagged *Pst* DC3000. (A) At 24hpi, whole seedlings were fixed and cleared using ClearSee. Green asterisks indicate stomata. Left: A single image of bright field channel. Middle: Maximum projections of Z stack of mVENUS and mCherry signals. Right: Merged image. Scale bar: 20 µm.

(B) Percentage of *FRK1* expressing cells surrounding a substomatal cavity (+) or not (-) at 24hpi. Boxplot shows median with minimum and maximum values indicated (n = 7 images from 4 plants). ****$p < 0.0001$ analyzed by two-tailed, unpaired Student's t-test. The experiment was repeated twice with similar results.

(C) Percentage of *FRK1* expressing cells that are proximal (<15 µm) or distal (>15 µm) to a bacterial colony 24hpi. Data was analyzed as described in (B).

(D) The immune marker *CBP60g* is expressed in skirt cells at the trichome base before inoculation and broadly expressed after infection. *Arabidopsis pCBP60g::NLS-3xmCitrine* seedlings were inoculated as described in (A). Representative images of *CBP60g* expression at 24h in mock or DC3000-treated samples. Maximum projections of a Z stack of mCitrine signals were combined with a single image of chlorophyll autofluorescence. Chlorophyll autofluorescence is shown in blue. Red asterisks indicate skirt cells at the base of trichomes. Scale bars: 200 µm, and 50 µm in inset.

(E) Number of *CBP60g* expressing cells at 24h in mock- or DC3000-treated samples. Boxplot shows median with minimum and maximum values indicated (n = 10 images from 5 plants). $p < 0.0001$, one-way ANOVA with Tukey test. The experiment was repeated twice with similar results.

(F) The susceptible marker *ILL5* is expressed in guard cells before inoculation and broadly expressed after infection. *Arabidopsis pILL5::NLS-3xmCitrine* seedlings were inoculated as described in (A). Representative images of *ILL5* expression at 48h in mock- or DC3000-treated samples. Maximum projections of Z stack of mCitrine signals were combined with single image of bright filed channel. Scale bar: 20 µm.

(G) Number of *ILL5* expressing cells at 24h in mock- or DC3000-treated samples. Boxplot shows median with minimum and maximum values indicated (n = 6 images from 3 plants). $p < 0.0001$, ANOVA with Tukey test. The experiment was repeated three times with similar results.

Figure 6

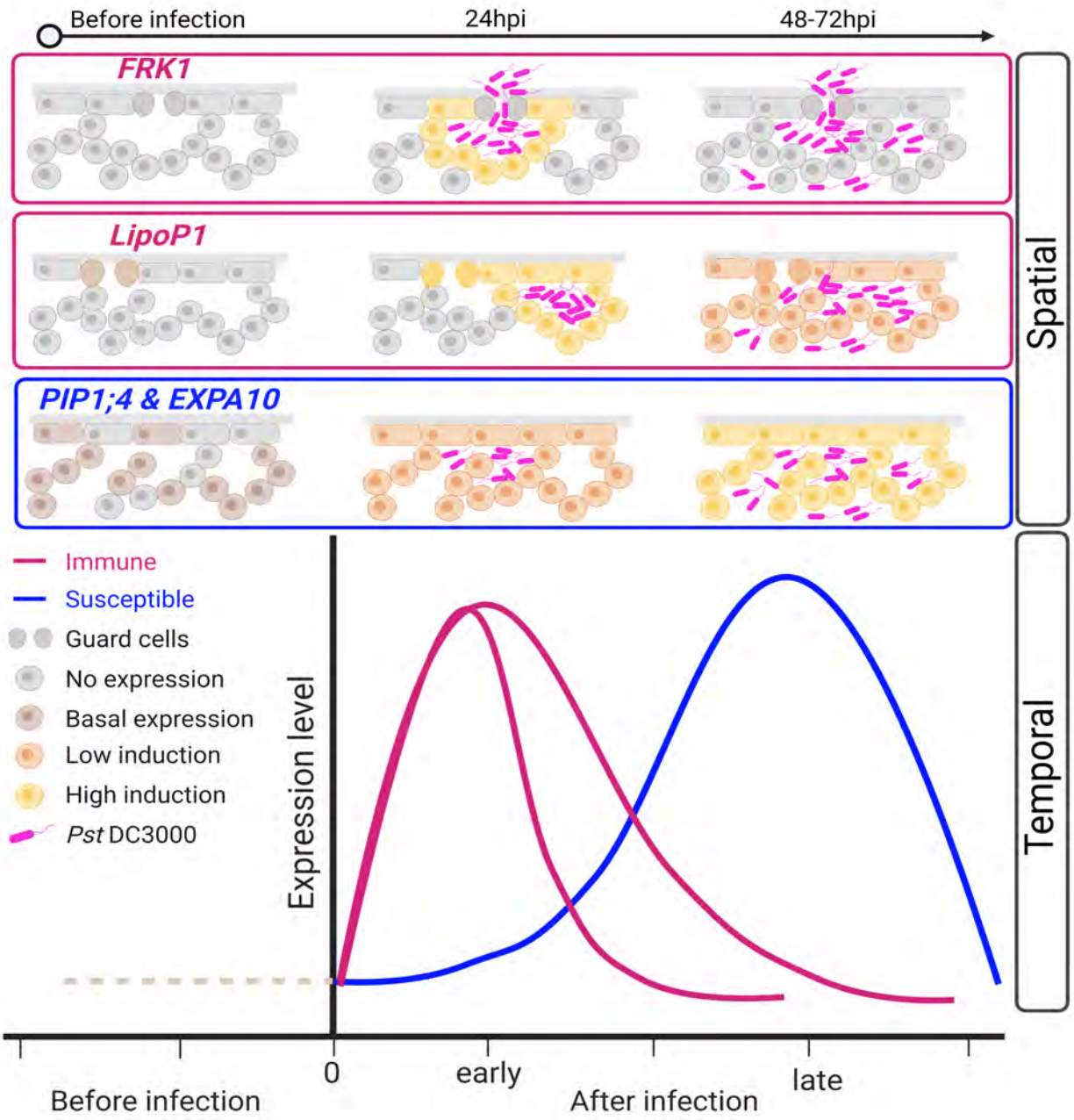

Figure 6. Spatial and temporal model of immune and susceptible marker gene expression.
Immune and susceptible cell cluster markers exhibit diverse spatial and temporal expression patterns. Immune markers are highly induced at early infection stages, with *FRK1* and *LipoP1* induction in close proximity to bacterial colonies. At later time points (48h), the *FRK1* marker is no longer expressed, while other immune markers including *LipoP1* exhibit more general expression patterns throughout the leaf. Susceptible cell cluster markers exhibit basal expression that is broadly induced after infection throughout the leaf and peaks at late stages. Created with BioRender.com

Figure S1

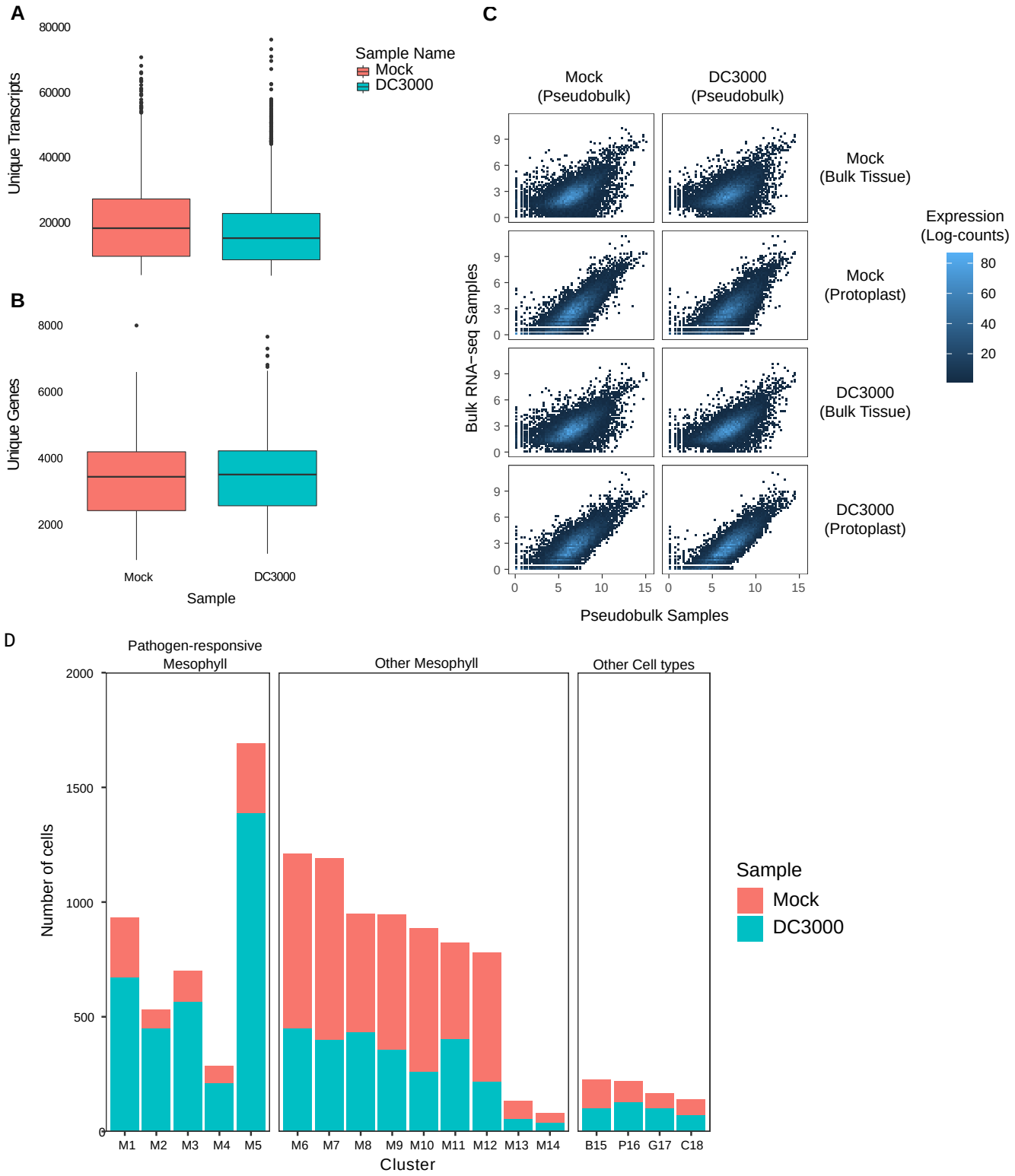

Figure S1. Summary statistics of single-cell datasets, and comparison with bulk RNA-seq. Related to Figure 1-2.

Transcript (A) and Gene (B) counts were summarized across all 11,895 cells in the integrated single-cell dataset. Median transcript counts were ~ 17,000 unique molecular identifier (UMI) per cell for both datasets, while median gene counts were ~ 3,500. (C) For Mock- and DC3000-treated single-cell datasets, a “pseudobulk” profile was calculated as the sum of counts per gene for all cells within that dataset. These profiles were compared to mRNA-seq data derived from whole leaves (Bulk Tissue) and pooled protoplasts (Protoplast) isolated in the same manner as those used for single-cell profiling). (D) Cell numbers from *Arabidopsis* leaves infiltrated with *Pst* DC3000 or 10mM $MgCl_2$ (Mock) in each cluster.

Figure S2

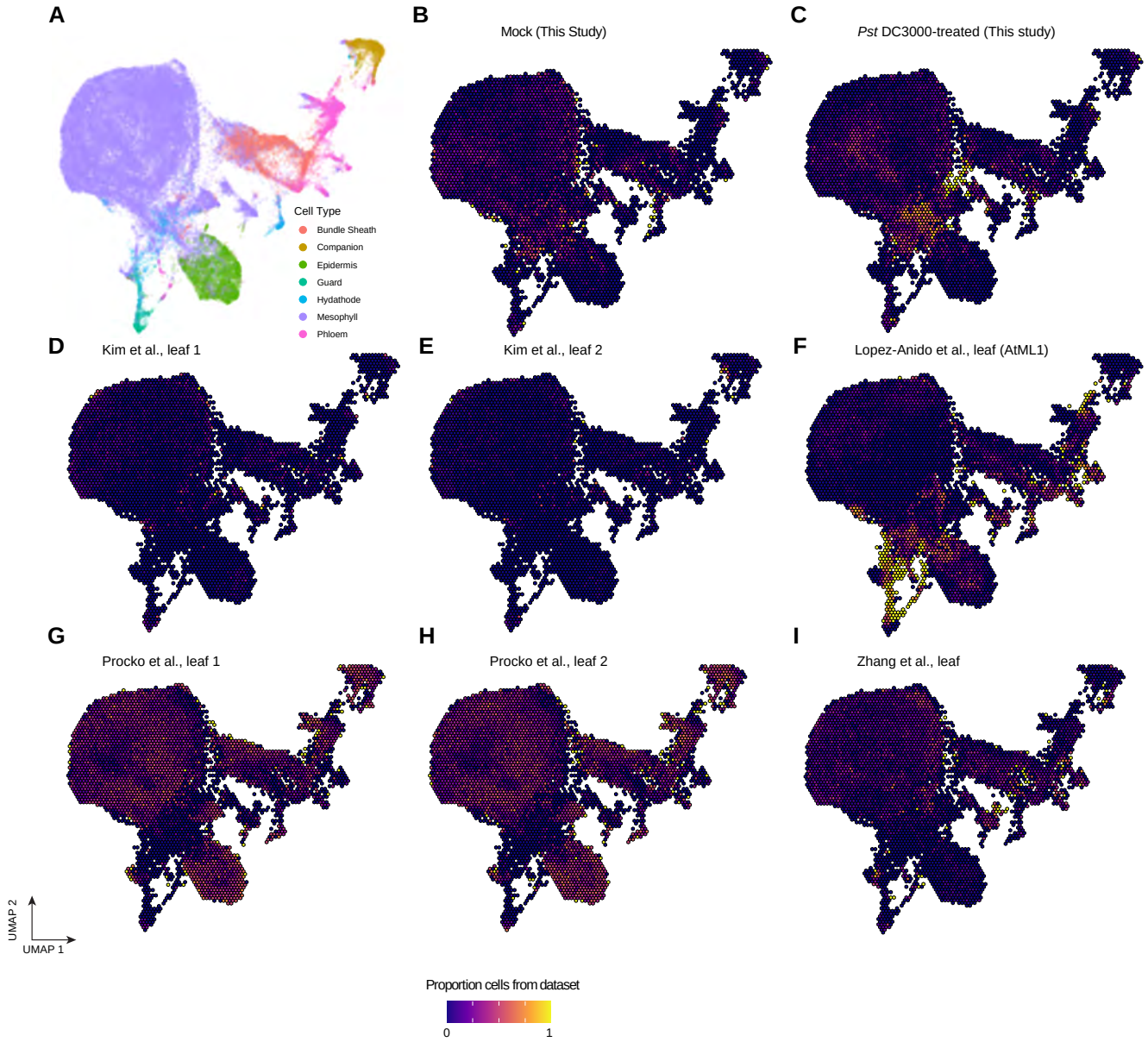

Figure S2. Integration of five leaf single-cell datasets from *Arabidopsis* preserves the unique identity of pathogen-treated cells. Related to Figure 1.

We integrated *Arabidopsis* leaf single-cell datasets (eight total, over five distinct studies: Kim et al., 2021; Liu et al., 2020; Lopez-Anido et al., 2021; Procko et al., 2022; Zhang et al., 2019) together to determine whether pathogen-treated cells remain distinct relative to other sources of cell-cell variation. (A) Cell type distribution in UMAP space for the integrated dataset. (B-H) Proportion of cells in UMAP space belonging to each individual dataset. While the combination of all datasets largely preserved clustering with respect to cell type (A), a region in UMAP space still appeared to be distinct for having *Pst* 3000-treated identity (C). Heatmap represents proportion of cells for each dataset overlaid onto the integrated UMAP.

Figure S3

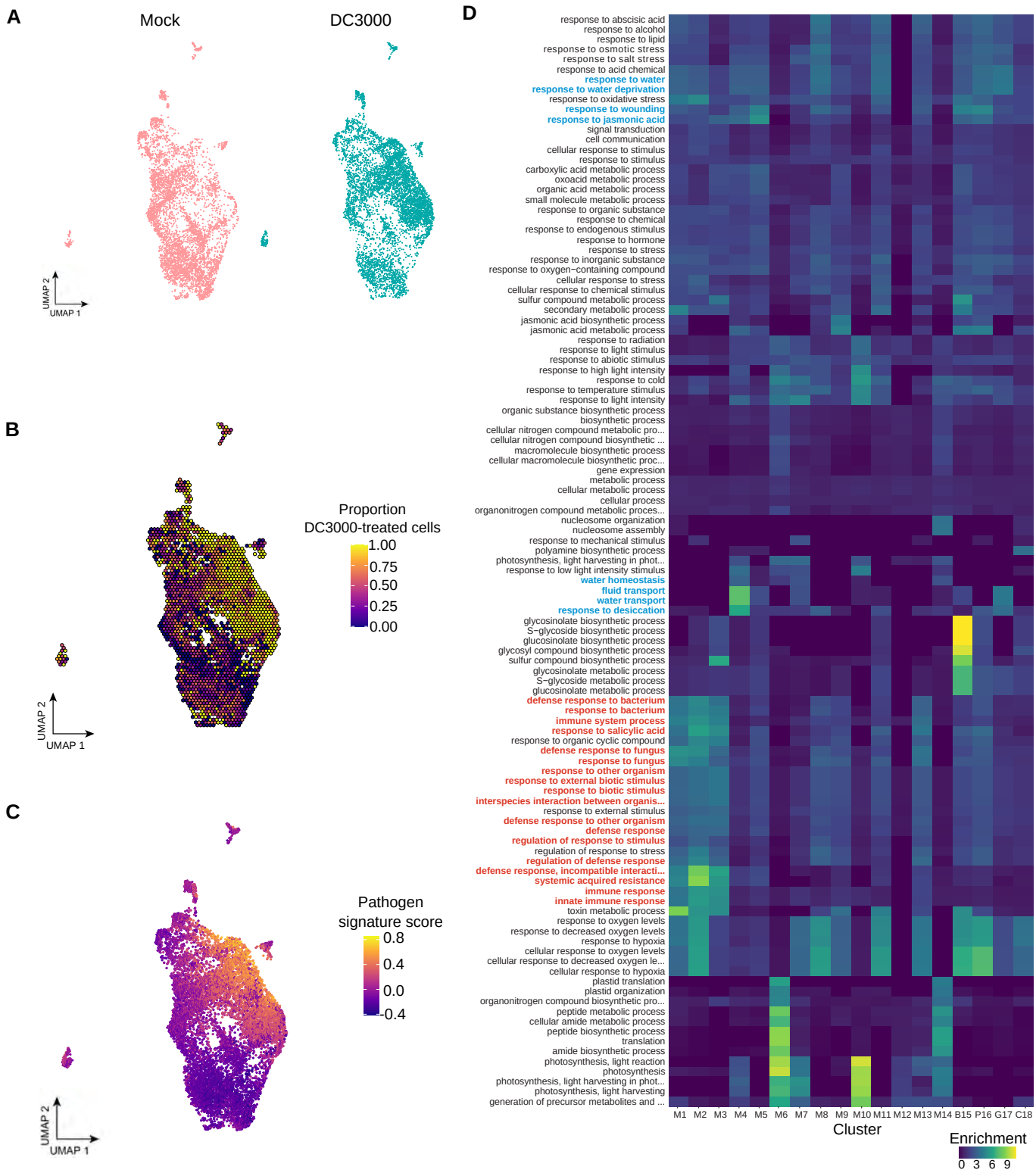
A
Mock
DC3000
UMAP 2
UMAP 1
B
Proportion
DC3000-treated cells
1.00
0.75
0.50
0.25
0.00
UMAP 2
UMAP 1
C
Pathogen
signature score
0.8
0.4
0.0
-0.4
UMAP 2
UMAP 1
D
response to abscisic acid
response to alcohol
response to lipid
response to osmotic stress
response to salt stress
response to acid chemical
response to water
response to water deprivation
response to oxidative stress
response to wounding
response to jasmonic acid
signal transduction
cell communication
cellular response to stimulus
response to stimulus
carboxylic acid metabolic process
oxoacid metabolic process
organic acid metabolic process
small molecule metabolic process
response to organic substance
response to chemical
response to endogenous stimulus
response to hormone
response to stress
response to inorganic substance
response to oxygen−containing compound
cellular response to stress
cellular response to chemical stimulus
sulfur compound metabolic process
secondary metabolic process
jasmonic acid biosynthetic process
jasmonic acid metabolic process
response to radiation
response to light stimulus
response to abiotic stimulus
response to high light intensity
response to cold
response to temperature stimulus
response to light intensity
organic substance biosynthetic process
biosynthetic process
cellular nitrogen compound metabolic pro...
cellular nitrogen compound biosynthetic ...
macromolecule biosynthetic process
cellular macromolecule biosynthetic proc...
gene expression
metabolic process
cellular metabolic process
cellular process
organonitrogen compound metabolic proces...
nucleosome organization
nucleosome assembly
response to mechanical stimulus
polyamine biosynthetic process
photosynthesis, light harvesting in phot...
response to low light intensity stimulus
water homeostasis
fluid transport
water transport
response to desiccation
glycosinolate biosynthetic process
S−glycoside biosynthetic process
glucosinolate biosynthetic process
glycosyl compound biosynthetic process
sulfur compound biosynthetic process
glycosinolate metabolic process
S−glycoside metabolic process
glucosinolate metabolic process
defense response to bacterium
response to bacterium
immune system process
response to salicylic acid
response to organic cyclic compound
defense response to fungus
response to fungus
response to other organism
response to external biotic stimulus
response to biotic stimulus
interspecies interaction between organis...
response to external stimulus
defense response to other organism
defense response
regulation of response to stimulus
regulation of response to stress
regulation of defense response
defense response, incompatible interacti...
systemic acquired resistance
immune response
innate immune response
toxin metabolic process
response to oxygen levels
response to decreased oxygen levels
response to hypoxia
cellular response to oxygen levels
cellular response to decreased oxygen le...
cellular response to hypoxia
plastid translation
plastid organization
organonitrogen compound biosynthetic pro...
peptide metabolic process
cellular amide metabolic process
peptide biosynthetic process
translation
amide biosynthetic process
photosynthesis, light reaction
photosynthesis
photosynthesis, light harvesting in phot...
photosynthesis, light harvesting
generation of precursor metabolites and ...
M1 M2 M3 M4 M5 M6 M7 M8 M9 M10 M11 M12 M13 M14 B15 P16 G17 C18
Cluster
Enrichment
0 3 6 9

Figure S3. Clusters M1 – M5 are pathogen-responsive clusters. Related to Figure 2.

(A) Single Cell Uniform Manifold Approximation and Projection (UMAP) plots from mock-treated samples (Mock) and *Pst* DC30000-treated samples, colored according to treatment. (B) Proportion of DC3000-treated cells is depicted in the UMAP of the combined single-cell RNA-seq datasets. These cells likely represent those that are responsive to pathogen infection. (C) A *Pst* DC3000 signature score was computed as a composite metric quantifying the overall impact that *P. syringae* has on each cell (Methods). The pathogen signature score is depicted in the UMAP of the combined scRNA-seq datasets. (D) GO-term enrichment (number of significant genes divided by the number of expected genes for each term) shows many terms specific to immunity and defense (bold, red) are associated with clusters M1-3, while terms specific to jasmonic acid, wounding and water stress (blue) are associated with clusters M4-5.

Figure S4

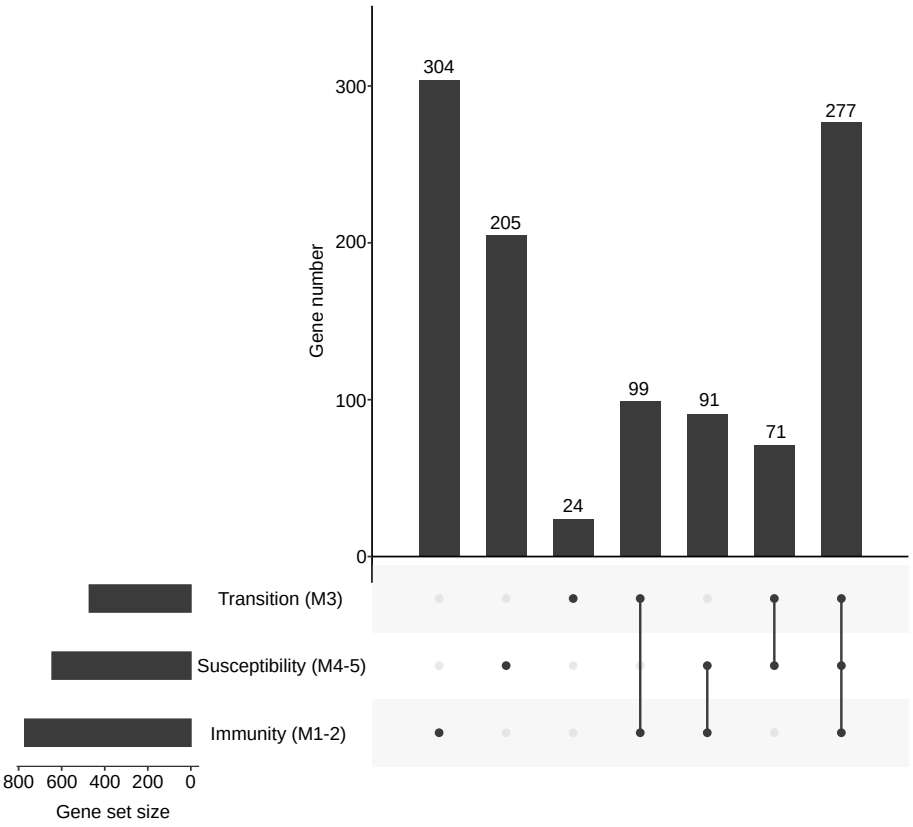

Figure S4. Overlap and specificity of differentially expressed genes in pathogen responsive clusters. Related to Figure 2.

Overlap among genes identified as differentially expressed among different pathogen-responsive mesophyll cell types in single-cell data (log2-fold change > 0.5, adjusted p-value < 0.01, and negative binomial test using DESeq2).

Figure S5

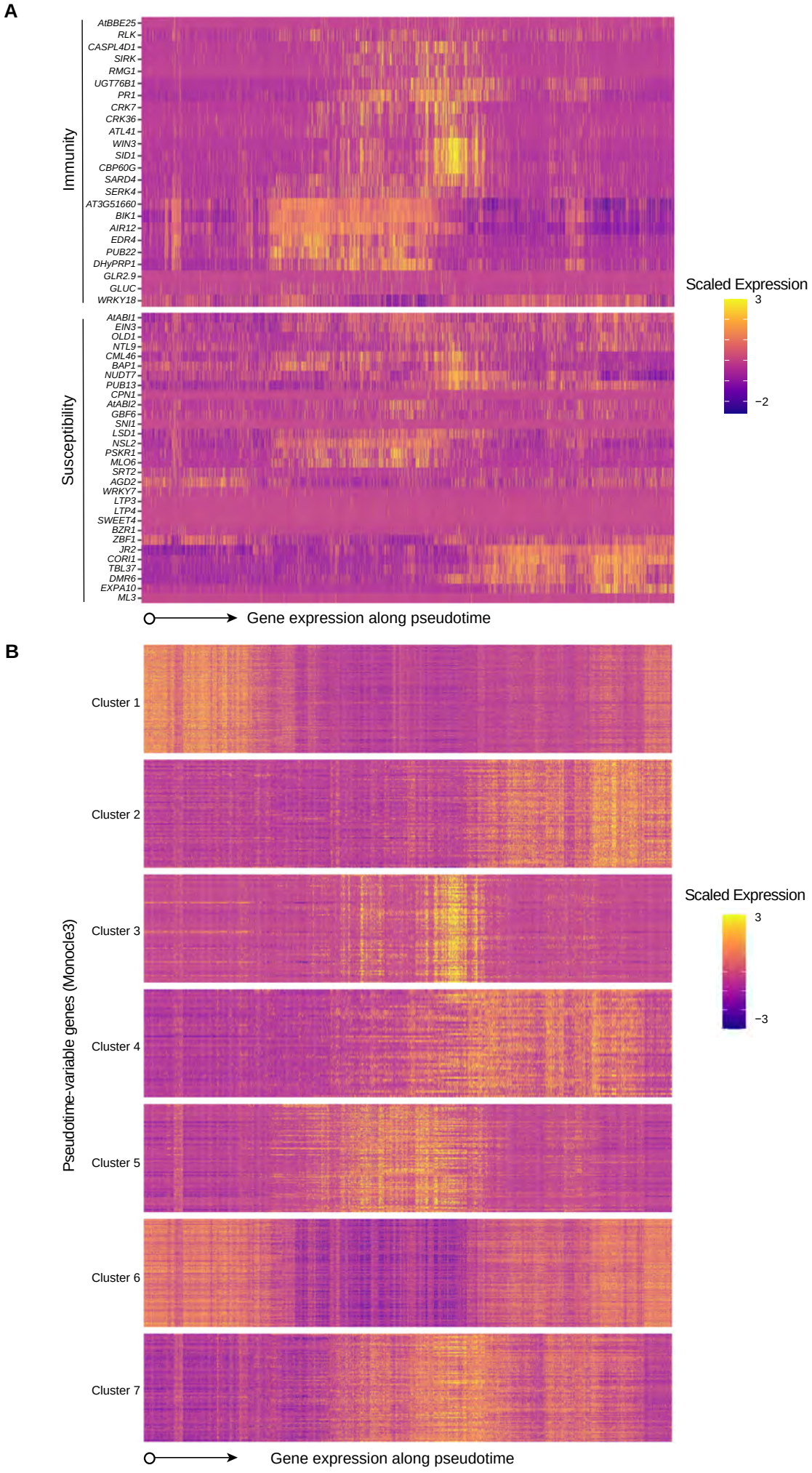
A
Immunity
AtBBE25
RLK
CASPL4D1
SIRK
RMG1
UGT76B1
PR1
CRK7
CRK36
ATL41
WIN3
SID1
CBP60G
SARD4
SERK4
AT3G51660
BIK1
AIR12
EDR4
PUB22
DHyPRP1
GLR2.9
GLUC
WRKY18
Susceptibility
AtABI1
EIN3
OLD1
NTL9
CML46
BAP1
NUDT7
PUB13
CPN1
AtABI2
GBF6
SNI1
LSD1
NSL2
PSKR1
MLO6
SRT2
AGD2
WRKY7
LTP3
LTP4
SWEET4
BZR1
ZBF1
JR2
CORI1
TBL37
DMR6
EXPA10
ML3
Scaled Expression
3
−2
Gene expression along pseudotime
B
Pseudotime-variable genes (Monocle3)
Cluster 1
Cluster 2
Cluster 3
Cluster 4
Cluster 5
Cluster 6
Cluster 7
Scaled Expression
3
−3
Gene expression along pseudotime

Figure S5. Variation of known and novel pathogen-responsive genes along pseudotime. Related to Figure 2 and Table S3.

(A) Expression is shown for genes known to be involved in pathogen responsiveness. Known genes are organized based on their suspected involvement in immunity (top) or in disease susceptibility (bottom) and expression in individual cells are depicted varying along pseudotime on the x-axis. (B) Novel clusters of genes exhibiting similar expression patterns that vary with pseudotime were identified using monocle3. Novel genes are organized based on a hierarchical clustering of scaled expression profiles over pseudotime. Y-axis represents individual genes within a cluster, and the X-axis represents expression in individual cells organized along pseudotime.

Figure S6

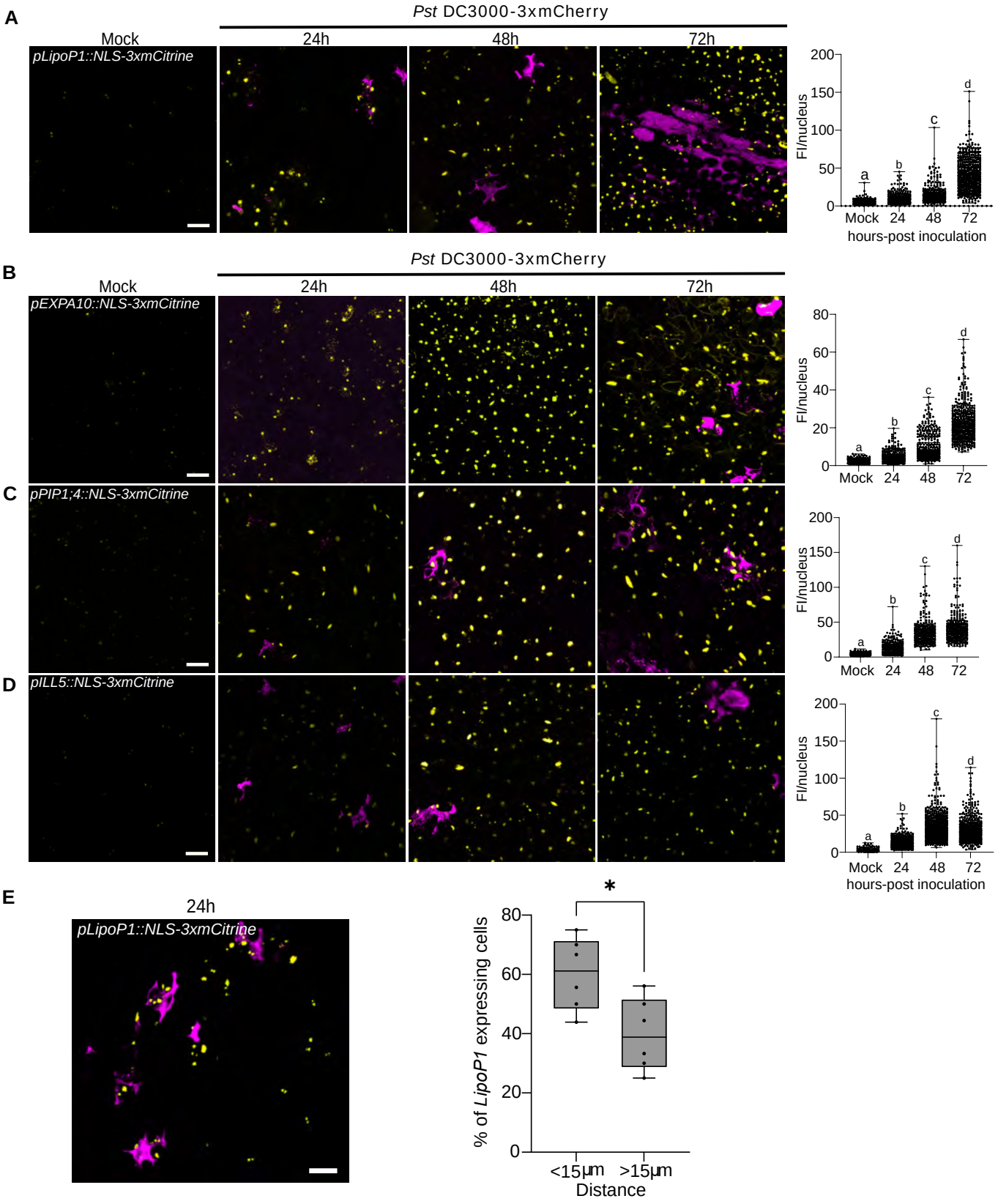
A
Pst DC3000-3xmCherry
Mock
24h
48h
72h
pLipoP1::NLS-3xmCitrine
FI/nucleus
hours-post inoculation
B
pEXPA10::NLS-3xmCitrine
C
pPIP1;4::NLS-3xmCitrine
D
pILL5::NLS-3xmCitrine
E
pLipoP1::NLS-3xmCitrine
% of LipoP1 expressing cells
<15µm
>15µm
Distance

Figure S6. Visualization of immune and susceptible cellular markers during disease progression. Related to Figure 3-5.

Data represent experiments with a second, independent transgenic line for promoter-reporter constructs (line 2). (A) The immune marker *LipoP1* is highly expressed during infection. The promoter-reporter line for this immune marker was generated with fusion to 3xfluorophore possessing a nuclear localization signal (NLS). Two-week-old transgenic *Arabidopsis* seedlings grown on Murashige-Skoog plates were surface-inoculated with mCherry-tagged *Pst* DC3000 at concentration of 1 x 10^7 colony forming units/ml (CFU/ml). Left: Representative images of *LipoP1* expression at different infection stages. Mock images are taken at 24h. Pictures are maximum projections from confocal Z stacks. Right: Mean florescence intensity (FI, mean gray values) per nucleus was calculated and boxplot shows median with minimum and maximum values indicated (n = 6 images from 3 plants). Different letters indicate statistically significant differences ($p < 0.0001$, ANOVA with Tukey test). Scale bars: 50 µm. All experiments were repeated at least two times with similar results.

(B, C and D) The susceptible markers *EXPA10* (B), *PIP1;4* (C) and *ILL5* (D) are highly induced at late infection stages. Promoter-reporter lines for each susceptible marker were generated as mentioned in (A). Left: Representative images of susceptible marker expression at different infection stages. Plants were inoculated as described in (A) and mock images are taken at 24h. Pictures are maximum projections from confocal Z stacks. Right: Mean florescence intensity (mean gray values) per nucleus was calculated and boxplot shows median with minimum and maximum values indicated (n = 6 images from 3 plants). Different letters indicate statistically significant differences ($p < 0.0001$, ANOVA with Tukey test). All experiments were repeated at least two times with similar results. Scale bars: 50 µm.

(E) Expression of *LipoP1* is proximal to bacterial colonies at 24hpi of *Pseudomonas* infection. Left: Confocal micrograph of representative images of *Pst* DC3000-inoculated *Arabidopsis* leaves at 24hpi. Scale bars: 50 µm. Right: Percentage of *LipoP1* expressing cells that are proximal (<15 µm) or distal (>15 µm) to a bacterial colony 24hpi. Boxplot shows median with minimum and maximum values indicated (n = 6 images from 3 plants). ****$p < 0.0001$ analyzed by two-tailed, unpaired Student's t-test. Experiment was repeated three times with similar results.